Monthly Notices of the ROYAL ASTRONOMICAL SOCIETY

MNRAS **524,** 5929–5943 (2023)
Advance Access publication 2023 July 26

https://doi.org/10.1093/mnras/stad2248

General relativistic pulsations of ultra-massive ZZ Ceti stars

Alejandro H. Córsico,[1,2]★ S. Reece Boston,[3,4]★ Leandro G. Althaus,[1,2]★ Mukremin Kilic,[5] S. O. Kepler,[6] María E. Camisassa[7] and Santiago Torres[7,8]

[1]*Facultad de Ciencias Astronómicas y Geofísicas, Universidad Nacional de La Plata, Paseo del Bosque s/n, 1900 La Plata, Argentina*
[2]*Instituto de Astrofísica de La Plata, UNLP-CONICET, Paseo del Bosque s/n, 1900 La Plata, Argentina*
[3]*Department of Physics and Astronomy, University of North Carolina at Chapel Hill, Chapel Hill, NC 27599, USA*
[4]*Computer Science and Mathematics Division, Oak Ridge National Laboratory, Oak Ridge, TN 37830, USA*
[5]*Homer L. Dodge Department of Physics and Astronomy, University of Oklahoma, 440 W. Brooks St, Norman, OK 73019, USA*
[6]*Instituto de Física, Universidade Federal do Rio Grande do Sul, 91501-900 Porto Alegre RS, Brazil*
[7]*Departament de Física, Universitat Politécnica de Catalunya, c/ Esteve Terrades 5, E-08860 Castelldefels, Spain*
[8]*Institute for Space Studies of Catalonia, c/Gran Capita 2–4, Edif. Nexus 104, E-08034 Barcelona, Spain*

Accepted 2023 July 20. Received 2023 July 20; in original form 2023 June 2

ABSTRACT

Ultra-massive white dwarf stars are currently being discovered at a considerable rate, thanks to surveys such as the *Gaia* space mission. These dense and compact stellar remnants likely play a major role in Type Ia supernova explosions. It is possible to probe the interiors of ultra-massive white dwarfs through asteroseismology. In the case of the most massive white dwarfs, general relativity could affect their structure and pulsations substantially. In this work, we present results of relativistic pulsation calculations employing relativistic ultra-massive ONe-core white dwarf models with hydrogen-rich atmospheres and masses ranging from 1.29 to 1.369 $M_\odot$ with the aim of assessing the impact of general relativity on the adiabatic gravity (g)-mode period spectrum of very high mass ZZ Ceti stars. Employing the relativistic Cowling approximation for the pulsation analysis, we find that the critical buoyancy (Brunt–Väisälä) and acoustic (Lamb) frequencies are larger for the relativistic case, compared to the Newtonian case, due to the relativistic white dwarf models having smaller radii and higher gravities for a fixed stellar mass. In addition, the g-mode periods are shorter in the relativistic case than those in the Newtonian computations, with relative differences of up to ∼50 per cent for the highest mass models (1.369 $M_\odot$) and for effective temperatures typical of the ZZ Ceti instability strip. Hence, the effects of general relativity on the structure, evolution, and pulsations of white dwarfs with masses larger than ∼1.29 $M_\odot$ cannot be ignored in the asteroseismological analysis of ultra-massive ZZ Ceti stars.

Key words: asteroseismology – relativistic processes – stars: evolution – stars: interiors – stars: oscillations – white dwarfs.

1 INTRODUCTION

ZZ Ceti variables are pulsating DA (H-rich atmosphere) white dwarf (WD) stars with effective temperatures in the range 10 500 K $\lesssim T_{\rm eff} \lesssim$ 13 500 K and surface gravities in the interval 7.5 $\lesssim \log g \lesssim$ 9.35. They exhibit periods from ∼100 to ∼1400 s due to non-radial gravity (g) modes with harmonic degrees $\ell = 1$ and $\ell = 2$ (Fontaine & Brassard 2008; Winget & Kepler 2008; Althaus et al. 2010). The interiors of these compact stars, which constitute the evolutionary end of most stars in the Universe, can be investigated through the powerful tool of asteroseismology by comparing the observed periods with theoretical periods computed using large grids of WD stellar models (e.g. Córsico et al. 2019).

Although most ZZ Ceti stars have masses between ∼0.5 and ∼0.8 $M_\odot$, at least seven ultra-massive ($M_\star \gtrsim 1.05$ $M_\odot$) ZZ Ceti stars have been discovered so far: BPM 37093 ($M_\star = 1.13$ $M_\odot$; Kanaan et al. 1992; Bédard, Bergeron & Fontaine 2017), GD 518 ($M_\star = 1.24$ $M_\odot$; Hermes et al. 2013), SDSS J084021.23+522217.4 ($M_\star = 1.16$ $M_\odot$; Curd et al. 2017), WD J212402.03−600100.05 ($M_\star = 1.16$ $M_\odot$; Rowan et al. 2019), J0204+8713 and J0551+4135 ($M_\star = 1.05$ $M_\odot$ and $M_\star = 1.13$ $M_\odot$, respectively; Vincent, Bergeron & Lafrenière 2020), and WD J004917.14−252556.81 ($M_\star \sim$ 1.30 $M_\odot$; Kilic et al. 2023b). With such a high stellar mass, the latter is the most massive pulsating WD currently known. The discovery and characterization of pulsating ultra-massive WDs through asteroseismology is important for understanding the supernovae Type Ia explosions. We know that accreting CO-core WDs are the progenitors of these explosions (e.g. Nugent et al. 2011; Maoz, Mannucci & Nelemans 2014), but we have not been able to probe the interior structure of such WDs near the Chandrasekhar limit.

Modern photometric data of pulsating WDs collected by spacecrafts, such as the ongoing *Transiting Exoplanet Survey Satellite* (*TESS*) mission (Ricker et al. 2014) and the already finished *Kepler*/*K2* space mission (Borucki et al. 2010; Howell et al. 2014), brought along revolutionary improvements to the field of WD asteroseismology in at least two aspects (Córsico 2020, 2022). First, the space missions provide pulsation periods with an unprecedented precision. Indeed, the observational precision limit of *TESS* for the pulsation periods is of the order of $\sim 10^{-4}$ s or even smaller (Giammichele, Charpinet & Brassard 2022). Secondly, these space

★ E-mail: acorsico@fcaglp.unlp.edu.ar (AHC); rboston@live.unc.edu (SRB); althaus@fcaglp.unlp.edu.ar (LGA)

© 2023 The Author(s)
Published by Oxford University Press on behalf of Royal Astronomical Society

Downloaded from https://academic.oup.com/mnras/article/524/4/5929/7231806 by guest on 07 August 2023

missions also enable the discovery of large numbers of new pulsating WDs. For example, Romero et al. (2022) used the *TESS* data from the first 3 yr of the mission, for Sectors 1 through 39, to identify 74 new ZZ Ceti stars, which increased the number of already known ZZ Cetis by ∼20 per cent. It is likely that many more pulsating WDs, not only average-mass ($M_\star \sim 0.60\,M_\odot$) objects but also ultra-massive WDs, will be identified by *TESS* and other future space telescopes such as the *Ultraviolet Transient Astronomy Satellite* (*ULTRASAT*; Ben-Ami et al. 2022) in the coming years, though *TESS*'s relatively small aperture limits its ability to observe intrinsically fainter massive WDs. In addition, large-scale wide-field ground-based photometric surveys like the Vera C. Rubin Observatory's Legacy Survey of Space and Time and the BlackGEM (Groot et al. 2022) will significantly increase the population of WD pulsators, including massive WDs.

The use of space telescopes for WD asteroseismology has opened up a new window into the interiors of these stars and led to some new and interesting questions. For example, the availability of pulsation periods with high precision supplied by modern space-based photometric observations has, for the first time, raised the question of whether it is possible to detect very subtle effects in the observed period patterns, such as the signatures of the current experimental $^{12}C(\alpha,\gamma)^{16}O$ reaction rate probability distribution function (Chidester, Farag & Timmes 2022), or the possible impact of general relativity (GR) on the pulsation periods of ZZ Ceti stars (Boston, Evans & Clemens 2023). In particular, the possibility that relativistic effects can be larger than the uncertainties in the observed periods when measured with space missions has led Boston et al. (2023) to conclude that, for average-mass WDs, the relative differences between periods in the Newtonian and relativistic calculations can be larger than the observational precision with which the periods are measured. Hence, to fully exploit the unprecedented quality of the observational data from *TESS* and similar space missions, it is necessary to take into account the GR effects on the structure and pulsations of WDs.

The impact of GR is stronger as we consider more massive WD configurations, in particular WDs with masses close to the Chandrasekhar mass ($M_{\rm Ch} \sim 1.4\,M_\odot$). Carvalho, Marinho & Malheiro (2018), Nunes, Arbañil & Malheiro (2021), and Althaus et al. (2022) used static WD models and evolutionary ONe-core WD configurations, respectively, to explore the effects of GR on the structure of ultra-massive WDs. These investigations found that GR strongly impacts the radius and surface gravity of ultra-massive WDs. In addition, Althaus et al. (2022) found that GR leads to important changes in cooling ages and in mass–radius relationships when compared with Newtonian computations. Furthermore, Althaus et al. (2023) have extended the relativistic computations to CO-core ultra-massive WD models.

In this work, we aim to assess the impact of GR on the g-mode period spectra of ultra-massive ZZ Ceti stars with masses $\gtrsim$1.29 $M_\odot$. This is the lower limit for the WD mass from which the effects of GR begin to be relevant (Althaus et al. 2022). Our analysis is complementary to that of Boston et al. (2023), which is focused on average-mass pulsating DA WDs (∼0.60 $M_\odot$; the bulk of pulsating WD population). For these average-mass DA WDs, the difference of Newtonian physics and GR was shown to be of the order of the surface gravitational redshift $z \sim 10^{-4}$, though for stars with very high central concentration of mass this difference could be an order of magnitude larger. Since the ultra-massive WDs are highly centrally condensed, GR might be even more important for these objects. The study of ultra-massive WDs is of particular interest at present, given the increasing rate of discovery of these objects (Gagné et al. 2018; Hollands et al. 2020; Kilic et al. 2020, 2021, 2023a; Caiazzo et al. 2021; Torres et al. 2022) and the prospect of finding pulsating ultra-massive WDs more massive than WD J004917.14−252556.81 (Kilic et al. 2023b). This last point is particularly relevant in view of the capabilities of the current (e.g. *TESS*) and upcoming (e.g. *ULTRASAT*, LSST (Legacy Survey of Space and Time), and BlackGEM) surveys.

The formalism of stellar pulsations in GR began with Thorne & Campolattaro (1967), using the Regge–Wheeler gauge to treat the pulsations as linear perturbations on top of a static, spherically symmetric background (Regge & Wheeler 1957). The result was a reduction in the Einstein field equations (EFEs) that describe space-time curvature in GR to only five complex-valued equations for the perturbation amplitudes. Further theoretical work showed that this system was only fourth-complex-order, with two degrees of freedom describing the fluid perturbations and two describing the gravitational perturbations (Ipser & Thorne 1973). Later, Detweiler & Lindblom (1985) (see also Lindblom & Detweiler 1983) reduced the perturbed EFEs to the explicit form of four first-order complex-valued equations describing the normal mode perturbations. For quadrupole modes or higher ($\ell \geq 2$), the two gravitational degrees of freedom at the surface produce outgoing gravitational radiation (i.e. gravitational waves) that will gradually damp any excitations, so that stellar perturbations in GR can be at best quasi-normal.

In asteroseismology, the outgoing gravitational radiation is largely an undesired complication, requiring specialized methods to avoid carrying the boundary condition out to spatial infinity (Fackerell 1971; Chandrasekhar & Detweiler 1975; Andersson, Kokkotas & Schutz 1995; Lindblom, Mendell & Ipser 1997). The outgoing gravitational waves can be easily removed using a form of the Cowling approximation within GR, first developed by McDermott, van Horn & Scholl (1983) and further studied by Lindblom & Splinter (1990), McDermott et al. (1985), and Yoshida & Lee (2002). In this *relativistic Cowling* approximation, the gravitational degrees of freedom are set to zero, retaining only the fluid perturbations. Further, there is no intrinsic damping, so that the problem becomes real-valued and the modes are stationary. This treatment is widely used to study the pulsation and stability of compact stellar objects in situations where knowledge of the outgoing gravitational waves is irrelevant, and especially in stars with surface crystallization (Yoshida & Lee 2002; Flores, Hall & Jaikumar 2017). Another approach to include the relativistic effects in stellar pulsations is to use the post-Newtonian approximation (Cutler 1991; Poisson & Will 2014; Boston et al. 2023). This approach is able to include gravitational perturbations in the form of two scalar potentials and a vector potential, without also producing gravitational radiation (Boston 2022).

Most interest in pulsations of relativistic stars has focused on neutron stars (e.g. McDermott, van Horn & Hansen 1988; Lindblom & Splinter 1989a; Cutler & Lindblom 1992). The earliest calculations of pulsations in WDs involving GR tried to address the origin of radio sources discovered by Hewish et al. (1968), as an alternative to a neutron star origin (Thorne & Ipser 1968). These studies, which date back to the late 1960s, were devoted to computing the fundamental radial pulsation mode of Hamada–Salpeter WD models (Hamada & Salpeter 1961) including GR effects (Faulkner & Gribbin 1968; Skilling 1968; Cohen, Lapidus & Cameron 1969). Boston et al. (2023) have recently renewed interest in this topic by focusing on relativistic pulsations of ZZ Ceti stars and other pulsating WDs, concentrating on average-mass WDs. In this paper, we study the impact of GR on realistic evolutionary stellar models of ultra-massive DA WDs computed by Althaus et al. (2022), which are representative of very high mass ONe-core ZZ Ceti stars. As a first step, in this work

Downloaded from https://academic.oup.com/mnras/article/524/4/5929/7231806 by guest on 07 August 2023

we adopt the relativistic Cowling approximation described above to incorporate relativistic effects in the pulsation calculations, following the treatment provided in Yoshida & Lee (2002). In future papers, we plan to examine the post-Newtonian and full fourth-order GR equations, applied to ultra-massive ONe-core WDs and to ultra-massive CO-core WDs (Córsico et al., in preparation).

The paper is organized as follows. In Section 2, we briefly describe the relativistic WD models computed by Althaus et al. (2022), emphasizing the impact of GR on the stellar structure. We devote Section 3 to describe our approach for the relativistic non-radial stellar pulsations, particularly the formalism of the relativistic Cowling approximation (Sections 3.1, 3.2, 3.3, and 3.4). The pulsation results for our ultra-massive WD models are described in Section 4. Finally, in Section 5 we summarize our findings. We present in Appendix A a derivation of the relativistic version of the 'modified Ledoux' treatment of the Brunt–Väisälä frequency, and in Appendix B the results of a validation of the main results of the paper using a toy model based on Chandrasekhar's models.

2 RELATIVISTIC ULTRA-MASSIVE WD MODELS

To determine whether to employ GR or Newtonian gravity in a system like a star, a qualitative general criterion commonly used is to assess the magnitude of the 'relativistic correction factor', ε, defined as $\varepsilon = GM_\star/c^2R_\star$, where G is the Newtonian gravitational constant, c is the speed of light, and $M_\star$ and $R_\star$ are the stellar mass and radius, respectively (Poisson & Will 2014).[1] The larger the value of ε, the worse the approximation of Newtonian gravity. For instance, for a neutron star, ε is of the order of $\sim$0.1, while for a black hole, $\varepsilon \sim 1$. For average-mass ($\sim$0.6 $M_\odot$) WDs, ε is $\sim 10^{-4}$, and that is why until recently the relativistic effects have been neglected in the calculation of their structures. If we instead consider an ultra-massive WD star with $M \sim 1.3\,M_\odot$ and $\varepsilon \sim 0.001$, at first glance, it is not clear whether the relativistic effects should be included or not. However, Carvalho et al. (2018) showed that for the most massive WDs, the importance of GR for their structure and evolution cannot be ignored. In fact, numerous works based on static WD structures have shown that GR effects are relevant for the determination of the radius of massive WDs (Rotondo et al. 2011; Mathew & Nandy 2017; Carvalho et al. 2018; Nunes et al. 2021). In particular, these studies have demonstrated that for fixed values of mass, deviations of up to 50 per cent in the Newtonian WD radius are expected compared to the GR WD radius. Recently, Althaus et al. (2022) have presented the first set of constant-rest-mass ONe-core ultra-massive WD evolutionary models with masses greater than $\sim$1.30 $M_\odot$ (and up to 1.369 $M_\odot$) that fully take into account the effects of GR. This study demonstrates that the GR effects must be considered to assess the structural and evolutionary properties of the most massive WDs. This analysis has been extended recently by Althaus et al. (2023) to ultra-massive WDs with CO cores that result from the complete evolution of single progenitor stars that avoid C-ignition (Althaus et al. 2021; Camisassa et al. 2022).

Althaus et al. (2022) employed the LPCODE stellar evolution code, appropriately modified to take into account relativistic effects. They considered initial chemical profiles as predicted by the progenitor evolutionary history (Siess 2007, 2010; Camisassa et al. 2019), and computed model sequences of 1.29, 1.31, 1.33, 1.35, and 1.369 $M_\odot$

[1]The parameter ε is nothing more than the surface gravitational redshift in the Newtonian limit, z.

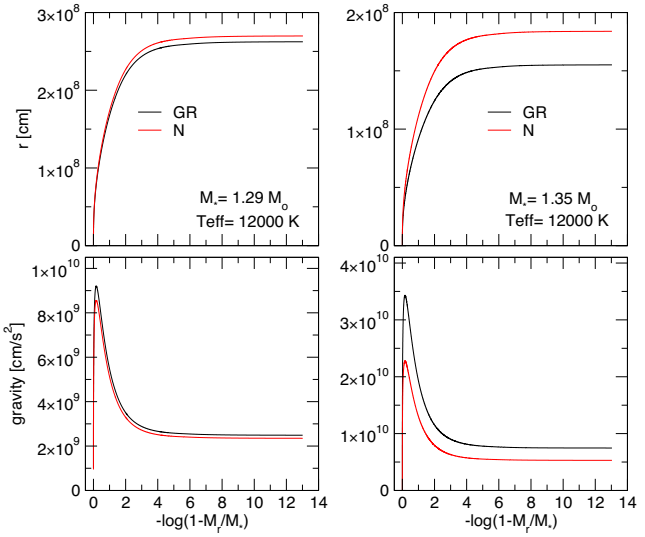

Figure 1. The stellar radius (upper panels) and gravity (bottom panels) in terms of the outer mass fraction coordinate corresponding to ultra-massive DA WD models with $M_\star = 1.29\,M_\odot$ (left) and $M_\star = 1.35\,M_\odot$ (right), the GR case (black curves) and the N case (red curves) ($T_{\rm eff} \sim 12\,000$ K).

WDs. The standard equations of stellar structure and evolution were generalized to include the effects of GR following Thorne (1977). In particular, the modified version of LPCODE computes the dimensionless GR correction factors $\mathscr{H}\mathscr{G}\mathscr{V}$ and $\mathscr{R}$, which turn to unity in the Newtonian limit. These factors correspond, respectively, to the enthalpy, gravitational acceleration, volume, and redshift correction parameters. For comparison purposes, Althaus et al. (2022) have also computed the same WD sequences for the Newtonian gravity case. All these sequences included the energy released during the crystallization process, both due to latent heat and the induced chemical redistribution, as in Camisassa et al. (2019).

We briefly describe below some of the properties of the representative models of ultra-massive ONe-core WD stars, emphasizing the impact of GR on their structure. We refer the reader to the paper by Althaus et al. (2022) for a detailed description of the effects of GR on the structural properties of these models. Here, we choose two template WD models characterized by stellar masses $M_\star = 1.29\,M_\odot$ and $M_\star = 1.35\,M_\odot$, H envelope thickness of $\log(M_{\rm H}/M_\star) \sim -6$, and an effective temperature of $T_{\rm eff} \sim 12\,000$ K, typical of the ZZ Ceti instability strip. We distinguish between two cases: one in which we consider Newtonian WD models (N case), and another one in which the WD structure is relativistic (GR case). In Fig. 1, we plot the run of the stellar radius and gravity in terms of the outer mass fraction coordinate, corresponding to WD models with $M_\star = 1.29\,M_\odot$ (left-hand panels) and $M_\star = 1.35\,M_\odot$ (right-hand panels), for the GR case (black curves) and the N case (red curves). Clearly, GR induces smaller radii and larger gravities, and this effect is much more pronounced for larger stellar masses.

In Table 1, which is a shortened version of table 1 of Althaus et al. (2022), we include the values of the stellar radius and the surface gravity for models with $T_{\rm eff} = 10\,000$ K and masses between 1.29 and 1.369 $M_\odot$ in the GR and N cases. As can be seen, the impact of GR on the radius and gravity of the models is noticeable. In Fig. 2, we plot the relative differences $\Delta R_\star = |R_\star^{\rm GR} - R_\star^{\rm N}|/R_\star^{\rm GR}$ (left-hand panel) and $\Delta g = (g^{\rm GR} - g^{\rm N})/g^{\rm GR}$ (right-hand panel) in terms of the stellar mass. The stellar radius is lower by $\sim$3 per cent (1.29 $M_\odot$) to $\sim$34 per cent (1.369 $M_\odot$), and the surface gravity is higher by

Downloaded from https://academic.oup.com/mnras/article/524/4/5929/7231806 by guest on 07 August 2023

Table 1. Stellar masses, radii, and surface gravities of the ultra-massive ONe-core WD models at $T_{\rm eff} = 10\,000$ K in the relativistic and Newtonian cases.

$M_\star/M_\odot$	$R_\star^{\rm GR}$ ($\times 10^8$ cm)	$R_\star^{\rm N}$ ($\times 10^8$ cm)	$\log g^{\rm GR}$ (cm s^{-2})	$\log g^{\rm N}$ (cm s^{-2})
1.29	2.609	2.685	9.401	9.375
1.31	2.326	2.426	9.507	9.470
1.33	2.005	2.157	9.643	9.579
1.35	1.543	1.829	9.878	9.728
1.369	1.051	1.409	10.217	9.961

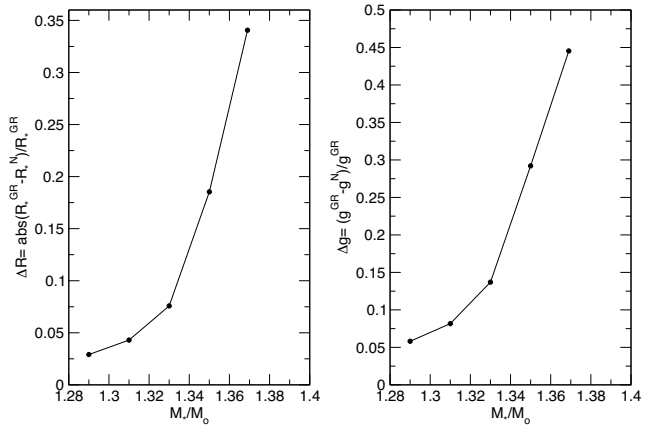

Figure 2. Left: the absolute relative difference between relativistic and Newtonian stellar radii versus stellar mass. Right: the relative difference between the relativistic and Newtonian surface gravities in terms of the stellar mass.

∼6 per cent (1.29 $M_\odot$) to ∼44 per cent (1.369 $M_\odot$) compared to the case where GR is neglected. The typical observational uncertainties in the radii and surface gravities of the most massive WDs in the Montreal White Dwarf Database 100 pc sample (Kilic et al. 2021) are 3 and 6 per cent, respectively. Hence, the differences between the GR and N cases can be detected observationally for WDs with masses above ∼1.3 $M_\odot$. These discrepancies must have important consequences for the pulsational properties of ultra-massive WDs, as we will see in Section 4.2.

3 RELATIVISTIC NON-RADIAL STELLAR PULSATIONS IN WDS

In order to incorporate the relativistic effects in the pulsations of WDs, we adopt the relativistic Cowling approximation in the form developed by Yoshida & Lee (2002), and follow the GR formalism provided in Boston (2022).

3.1 The relativistic Cowling approximation

The Cowling approximation of Newtonian non-radial pulsations (named after T. G. Cowling's pioneer paper; Cowling 1941) is based on neglecting the gravitational potential perturbations during the fluid oscillations. This approximation has been widely used in Newtonian non-radial pulsation computations in the past, because it constitutes a second-order differential eigenvalue problem, thus simplifying the complete fourth-order problem (Unno et al. 1989). It is also a very good approximation to periods of g modes in WDs, which are primarily envelope modes (Montgomery et al. 1999). The Cowling approximation has been frequently used in asymptotic treatment of stellar pulsations (see, for instance, Tassoul 1980), and also in numerical treatments of g-mode pulsations in rapidly rotating WDs (e.g. Saio 2019; Kumar & Townsley 2023), although it has fallen out of use in the context of present-day numerical calculations of Newtonian non-radial stellar pulsations and asteroseismology. The relativistic Cowling approximation (McDermott et al. 1983), on the other hand, is generally employed in the field of pulsations of relativistic objects such as neutron stars (Lindblom & Splinter ; Yoshida & Lee 2002; Sotani & Takiwaki 2020) and hybrid (hadron plus quark matter phases) neutron stars (Tonetto & Lugones 2020; Zheng et al. 2023).

In the next sections, we first describe the relativistic correction factors involved in the pulsation problem. Then, we provide relativistic expressions to calculate the critical frequencies (Brunt–Väisälä and Lamb frequencies), after which we assess the coefficients of the pulsation differential equations in the relativistic Cowling form. Finally, we provide the two first-order differential equations to be solved, along with the boundary conditions of the eigenvalue problem.

3.2 Relativistic correction factors $\mathscr{R}$, $\mathscr{V}$, and potentials ν and λ

We start by considering the Schwarzschild metric of GR for space-time inside and around a star (Thorne 1977):

$$ds^2 = -e^{2\Phi/c^2}c^2dt^2 + \left(1 - \frac{2Gm}{c^2 r}\right)^{-1} dr^2 + r^2 d\Omega^2, \quad (1)$$

where m is the 'total mass inside radius r', which includes the rest mass, nuclear binding energy, internal energy, and gravity. Φ is a gravitational potential, which in the Newtonian limit $c \to \infty$ corresponds to the scalar Newtonian potential.

Following Thorne (1977) in his treatment of relativistic stellar interiors, it is convenient to write the metric in the form

$$ds^2 = -\mathscr{R}^2 c^2 dt^2 + \mathscr{V}^2 dr^2 + r^2 d\Omega^2, \quad (2)$$

where the redshift correction factor $\mathscr{R}$ and the volume correction factor $\mathscr{V}$ are defined as (Thorne 1977)

$$\mathscr{R} = e^{\Phi/c^2}, \quad \mathscr{V} = \left(1 - \frac{2Gm}{c^2 r}\right)^{-1/2}. \quad (3)$$

The metric is usually written also as a function of two relativistic gravitational potentials ν and λ (Oppenheimer & Volkoff 1939; Tolman 1939), so that

$$ds^2 = -e^{\nu} c^2 dt^2 + e^{\lambda} dr^2 + r^2 d\Omega^2. \quad (4)$$

Equating equations (1) and (4), we have

$$\nu = \frac{2\Phi}{c^2}, \quad \text{and} \quad \lambda = -\ln\left(1 - \frac{2Gm}{c^2 r}\right). \quad (5)$$

We obtain ν and λ in terms of the variables $\mathscr{R}$ and $\mathscr{V}$, which are the output of the relativistic LPCODE version (Althaus et al. 2022) by equating equations (2) and (4):

$$\mathscr{R}^2 = e^{\nu}, \quad \mathscr{V}^2 = e^{\lambda}, \quad (6)$$

so that

$$\nu = 2\ln\mathscr{R}, \quad \lambda = 2\ln\mathscr{V}. \quad (7)$$

In the Newtonian limit, we have $\mathscr{R} = e^{\nu/2} \to 1$ and $\mathscr{V} = e^{\lambda/2} \to 1$, so that $\nu, \lambda \to 0$.

Downloaded from https://academic.oup.com/mnras/article/524/4/5929/7231806 by guest on 07 August 2023

We compute the derivatives of ν and λ by calculating the numerical derivatives of $\mathscr{R}$ and $\mathscr{V}$ as

$$\nu' \equiv \frac{\mathrm{d}\nu}{\mathrm{d}r} = \frac{2}{\mathscr{R}}\left(\frac{\mathrm{d}\mathscr{R}}{\mathrm{d}r}\right), \quad \lambda' \equiv \frac{\mathrm{d}\lambda}{\mathrm{d}r} = \frac{2}{\mathscr{V}}\left(\frac{\mathrm{d}\mathscr{V}}{\mathrm{d}r}\right). \tag{8}$$

The numerical derivatives of $\mathscr{R}$ and $\mathscr{V}$, as well as ν' and λ', are usually noisy when computed following equation (8). To avoid this, we compute ν' and λ' by employing solutions to the EFE for the static, spherically symmetric distribution of matter, given by Tolman (1939) and Oppenheimer & Volkoff (1939) (see also Tooper 1964):

$$\mathrm{e}^{-\lambda}\left(\frac{1}{r^2} - \frac{\lambda'}{r}\right) - \frac{1}{r^2} = -\frac{8\pi G}{c^4}\rho c^2, \tag{9}$$

$$\mathrm{e}^{-\lambda}\left(\frac{1}{r^2} + \frac{\nu'}{r}\right) - \frac{1}{r^2} = \frac{8\pi G}{c^4}P, \tag{10}$$

$$\frac{1}{2}\mathrm{e}^{-\lambda}\left[\nu'' + \frac{1}{2}\left(\nu' - \lambda'\right)\left(\nu' + \frac{2}{r}\right)\right] = \frac{8\pi G}{c^4}P, \tag{11}$$

where P is the pressure and ρ is the mass-energy density (not just the mass density). With some rearranging, we can write

$$\lambda' = \frac{1}{r} + \left(\frac{8\pi G}{c^2}\rho r - \frac{1}{r}\right)\mathrm{e}^{\lambda}, \tag{12}$$

$$\nu' = -\frac{1}{r} + \left(\frac{8\pi G}{c^4}Pr + \frac{1}{r}\right)\mathrm{e}^{\lambda}, \tag{13}$$

$$\nu'' = \frac{16\pi G}{c^4}P\mathrm{e}^{\lambda} - \frac{1}{2}\left(\nu' - \lambda'\right)\left(\nu' + \frac{2}{r}\right) \equiv \frac{\mathrm{d}^2\nu}{\mathrm{d}r^2}. \tag{14}$$

To summarize, in our numerical treatment we employ equations (12) and (13) to compute λ' and ν' using the value of λ calculated with equation (7). We employ equation (14) to assess ν'' using λ, λ', and ν' derived above. The quantity ν'' is required to compute one of the coefficients of the pulsation differential equations (Section 3.4).

3.3 Relativistic adiabatic exponent, sound speed, and Lamb and Brunt–Väisälä frequencies

The relativistic adiabatic exponent, defined as $\Gamma_1 = \left(\frac{\partial \log P}{\partial \log n}\right)_{\mathrm{ad}}$, where n is the baryonic number density, can be expressed as (Meltzer & Thorne 1966; Thorne 1967)

$$\Gamma_1 = \frac{\rho + (P/c^2)}{P}\left(\frac{\partial P}{\partial \rho}\right)_{\mathrm{ad}} = \frac{\rho + (P/c^2)}{\rho}\left(\frac{\partial \log P}{\partial \log \rho}\right)_{\mathrm{ad}}. \tag{15}$$

This should be compared with the Newtonian case, where $\Gamma_1 = \left(\frac{\partial \log P}{\partial \log \rho}\right)_{\mathrm{ad}}$. The relativistic sound speed, v_{s}, is given by (Curtis 1950)

$$v_{\mathrm{s}}^2 = \frac{\Gamma_1 P}{\rho + (P/c^2)}, \tag{16}$$

whereas in the Newtonian case, $v_{\mathrm{s}}^2 = \left(\frac{\partial P}{\partial \rho}\right)_{\mathrm{ad}} = \Gamma_1 \frac{P}{\rho}$.

The squared Lamb and Brunt–Väisälä critical frequencies of the non-radial stellar pulsations, L_ℓ^2 and N^2, can be written as (Boston 2022)

$$L_\ell^2 = \ell(\ell+1)\frac{v_{\mathrm{s}}^2}{r^2}, \tag{17}$$

$$N^2 = \frac{c^2}{2r}\nu'\mathrm{e}^{-\lambda}\left[\frac{1}{\Gamma_1}\left(\frac{\mathrm{d}\log P}{\mathrm{d}\log r}\right) - \frac{\rho}{\rho + (P/c^2)}\left(\frac{\mathrm{d}\log \rho}{\mathrm{d}\log r}\right)\right]. \tag{18}$$

This expression for N^2 is analogous to the Newtonian version of N^2 for $g \rightarrow \frac{c^2}{2}\nu'$ and an additional relativistic correction factor $\mathrm{e}^{-\lambda}$.

The relativistic prescription given by equation (18) for the assessment of the Brunt–Väisälä frequency is not well defined numerically, due to the high degree of electronic degeneracy prevailing in the core of the ultra-massive WDs, similar to the case of Newtonian pulsations (Brassard et al. 1991). In particular, the use of equation (18) leads to unacceptable numerical noise of N, which can lead to miscalculations of the adiabatic g-mode periods. To avoid this problem, we employ a numerically convenient relativistic expression, analogous to the Newtonian recipe known as the *modified Ledoux* prescription (Tassoul, Fontaine & Winget 1990). The appropriate relativistic expression for N^2, which is derived in Appendix A, is

$$N^2 = \mathrm{e}^{-\lambda}\left(\frac{c^2}{2}\nu'\right)^2 \frac{\rho + (P/c^2)}{P}\frac{\chi_T}{\chi_n}\left[\nabla_{\mathrm{ad}} - \nabla + B\right], \tag{19}$$

where B is the Ledoux term, defined as

$$B = -\frac{1}{\chi_T}\sum_{i=1}^{M-1}\chi_{X_i}\frac{\mathrm{d}\ln X_i}{\mathrm{d}\ln P}, \tag{20}$$

M being the number of different atomic species with fractional abundances X_i that satisfy the constraint $\sum_{i=1}^{M-1} X_i + X_M = 1$. The compressibilities χ_T, χ_n, and χ_{X_i} are defined as, similar to the Newtonian problem,

$$\chi_T = \left(\frac{\partial \ln P}{\partial \ln T}\right)_{n,\{X_i\}}, \ \chi_n = \left(\frac{\partial \ln P}{\partial \ln n}\right)_{T,\{X_i\}}, \ \chi_{X_i} = \left(\frac{\partial \ln P}{\partial \ln X_i}\right)_{T,n}. \tag{21}$$

Using $(\mathrm{d}\ln\rho/\mathrm{d}\ln n) = (\rho + P/c^2)/\rho$ (equation 5.90 of Boston 2022; see also Thorne 1967), the compressibility χ_n can be computed as

$$\chi_n = \frac{\rho + (P/c^2)}{\rho}\chi_\rho, \tag{22}$$

where $\chi_\rho = \left(\frac{\partial \ln P}{\partial \ln \rho}\right)_{T,\{X_i\}}$. Here, ∇_{ad} and ∇ are the adiabatic and actual temperature gradients, respectively, defined as

$$\nabla_{\mathrm{ad}} = \left(\frac{\partial \ln T}{\partial \ln P}\right)_{\mathrm{ad},\{X_i\}}, \quad \nabla = \frac{\mathrm{d}\ln T}{\mathrm{d}\ln P}. \tag{23}$$

Equation (19) is completely analogous to the Newtonian expression for the squared Brunt–Väisälä frequency, $N^2 = g^2(\rho/P)(\chi_T/\chi_\rho)[\nabla_{\mathrm{ad}} - \nabla + B]$. In the relativistic formula, g has been replaced by $c^2\nu'/2$, and the ratio ρ/P becomes $(\rho + P/c^2)/P$. There is an additional relativistic factor, $\mathrm{e}^{-\lambda}$, and the compressibility χ_ρ is replaced by χ_n, where n is the baryonic number density.

3.4 Differential equations of the relativistic Cowling approximation

Here, we formulate the system of differential equations of the non-radial pulsations in the relativistic Cowling approximation form that results when we ignore Eulerian metric perturbations in the pulsation equations (McDermott et al. 1983). This reduces the fourth-complex-order problem of non-radial pulsations in GR to a second-real-order problem, which can be written as two real, first-order differential equations. Following Yoshida & Lee (2002), we define the dimensionless variables ω, y_1, and y_2, analogous to Dziembowski's variables in Newtonian pulsations (Dziembowski

Downloaded from https://academic.oup.com/mnras/article/524/4/5929/7231806 by guest on 07 August 2023

1971):[2]

$$\omega^2 = \frac{R_\star^3}{GM_\star}\sigma^2, \quad y_1 = \frac{\xi_r}{r}\mathrm{e}^{-\mathrm{i}\sigma t}, \quad y_2 = \xi_h C_1 \omega^2 \mathrm{e}^{-\mathrm{i}\sigma t}, \tag{24}$$

where ξ_r and ξ_h correspond to the Lagrangian radial and horizontal displacements, respectively. We also define the following dimensionless functions, analogous to Dziembowski's coefficients (Dziembowski 1971), calculated with respect to the stellar equilibrium model (Boston 2022):

$$V_g(r) = -\frac{1}{\Gamma_1}\left(\frac{\mathrm{d}\log P}{\mathrm{d}\log r}\right) = \frac{\rho + (P/c^2)}{\Gamma_1 P}\frac{rc^2}{2}\nu', \tag{25}$$

$$U_1(r) = 2 + r\frac{\nu''}{\nu'}, \tag{26}$$

$$U_2(r) = r\lambda', \tag{27}$$

$$C_1(r) = \frac{GM_\star}{c^2 R_\star^3}\frac{2r}{\nu'}\mathrm{e}^{-\nu}, \tag{28}$$

and (Thorne 1966)

$$A^*(r) = \frac{1}{\Gamma_1}\left(\frac{\mathrm{d}\log P}{\mathrm{d}\log r}\right) - \frac{\rho}{\rho + (P/c^2)}\left(\frac{\mathrm{d}\log \rho}{\mathrm{d}\log r}\right) = \frac{rN^2}{c^2\nu'/2}\mathrm{e}^{\lambda}. \tag{29}$$

In the Newtonian limit, A^*, V_g, and C_1 will limit to their conventional expressions (Unno et al. 1989). On the other hand, in the Newtonian limit we have that U_1 tends to U, which is defined in Unno et al. (1989), and $U_2 \to 0$. Using these definitions, and defining $x = r/R_\star$, the resulting differential equations for the relativistic Cowling approximation (McDermott et al. 1983; Lindblom & Splinter ; Yoshida & Lee 2002; Boston 2022) are

$$x\frac{\mathrm{d}y_1}{\mathrm{d}x} = \left(V_g - 3 + U_2\right) y_1 + \left(\frac{\ell(\ell+1)}{C_1\omega^2} - V_g\right) y_2, \tag{30}$$

$$x\frac{\mathrm{d}y_2}{\mathrm{d}x} = \left(\mathrm{e}^{\lambda} C_1\omega^2 - A^*\right) y_1 + \left(1 + A^* - U_1\right) y_2. \tag{31}$$

In the Newtonian limit, we have $\mathrm{e}^{\lambda} \to 1$ and $U_2 \to 0$, and the equations adopt exactly the form of the Newtonian Cowling approximation (Cowling 1941; Unno et al. 1989). The boundary conditions for this system of differential equations are at the stellar (fluid) centre ($x = 0$)

$$y_1 C_1\omega^2 - \ell y_2 = 0, \tag{32}$$

and at the stellar surface ($x = 1$)

$$y_1 - y_2 = 0, \quad \text{and} \quad y_1 = 1 \ \text{(normalization condition)}. \tag{33}$$

These are the same boundary conditions as for the Newtonian Cowling approximation.

For the ultra-massive WD models considered in this work, the stellar core is crystallized, so that the so-called hard-sphere boundary conditions (Montgomery et al. 1999) may be adopted, which exclude the g-mode oscillations from the solid core regions. In that case, equation (32) is replaced by the condition

$$y_1 = 0 \quad \text{and} \quad y_2 = \text{arbitrary}, \tag{34}$$

at the radial shell $x = x_{\rm crys}$ associated with the outward-moving crystallization front, instead of the centre of the star ($x = 0$). To maintain consistency between Newtonian and GR calculations and for a clean comparison, we assume the same internal boundary condition for the GR case as for the N case that the eigenfunctions are approximately zero in the solid core, and can be treated with a hard-sphere boundary condition.

In this work, to take into account the relativistic effects on g-mode pulsations of crystallized ultra-massive WD models, the LP-PUL pulsation code (Córsico & Althaus 2006) has been appropriately modified to solve the problem of relativistic pulsations in the Cowling approximation as given by equations (30) and (31), with boundary conditions given by equations (33) and (34).

[2]At variance with Boston (2022), we use σ for the physically meaningful oscillation frequency and ω for the dimensionless frequency, following Unno et al. (1989).

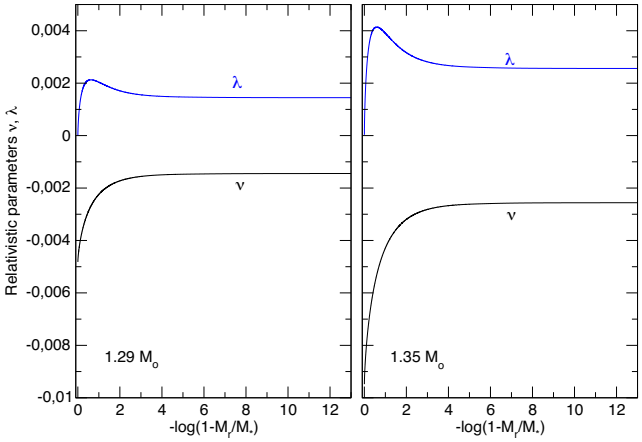

Figure 3. The relativistic potentials ν (black) and λ (blue), in terms of the outer mass fraction coordinate, corresponding to two template ONe-core WD models with masses $M_\star = 1.29\,\mathrm{M}_\odot$ and $M_\star = 1.35\,\mathrm{M}_\odot$, and effective temperature $T_{\rm eff} \sim 12\,000$ K. Note the high peaks in the stellar centre, indicating the increased gravitational strength of the core, and that the more massive star shows more extreme values. At the surface, $\nu \to -\lambda$.

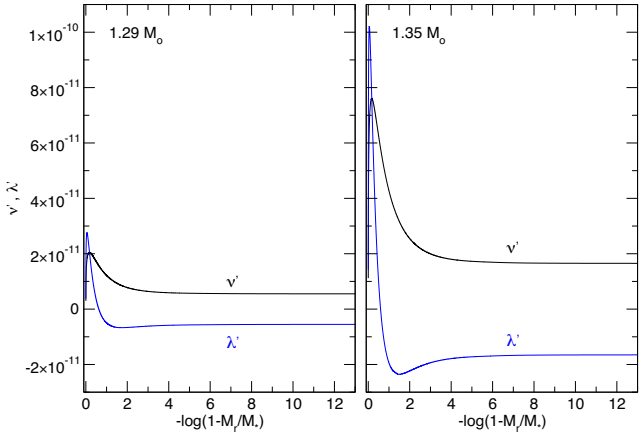

Figure 4. The derivatives of the relativistic potentials ν' (black) and λ' (blue), in terms of the outer mass fraction coordinate, corresponding to the same template models shown in Fig. 3. Note again the sharp peaks in the core, and more extreme values in the more massive star.

4 PULSATION RESULTS

4.1 Properties of template models

It is illustrative to examine the metric parameters ν, λ, ν', λ', and ν''. In Figs 3, 4, and 5, we show the ν and λ and their derivatives ν', λ', and ν'', in terms of the outer mass fraction coordinate, corresponding to the two template WD models with masses $M_\star = 1.29\,\mathrm{M}_\odot$ (left) and

Downloaded from https://academic.oup.com/mnras/article/524/4/5929/7231806 by guest on 07 August 2023

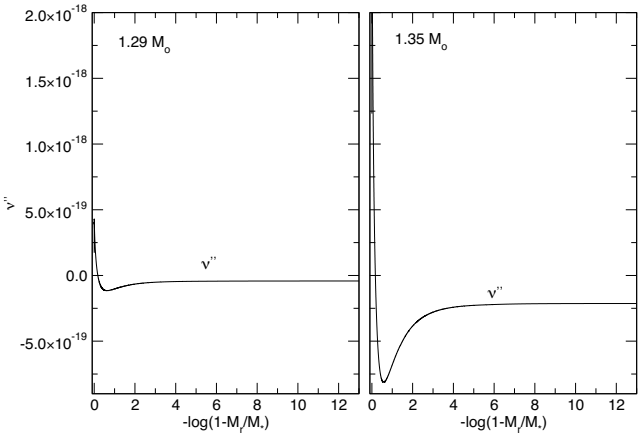

Figure 5. The second derivative of ν, that is, ν'', in terms of the outer mass fraction coordinate, corresponding to the same template models shown in Fig. 3.

$M_\star = 1.35\,\mathrm{M}_\odot$ (right), and effective temperature $T_{\rm eff} \sim 12\,000$ K. As can be seen, ν and λ quantities are very small throughout the star, being of a similar order with $\varepsilon \sim 0.001$. However, in the centre the gravitational values are more extreme than near the surface, pointing to the high central concentration of the mass of these stars.

The chemical profiles (abundances by mass, X_i) of the different nuclear species corresponding to the template models are plotted in the upper panels of Fig. 6 as a function of the fractional outer mass. In the lower panels, we depict the logarithm of the squared Brunt–Väisälä (black lines) and dipole ($\ell = 1$) Lamb (red lines) frequencies for the GR case (solid lines) and the N case (dashed lines). We have emphasized the crystallized regions of the core with grey. The chemical interface of ^{12}C, ^{16}O, and ^{20}Ne, which is located at $-\log(1 - M_r/M_\star) \sim 1.5$, is embedded in the crystalline part of the core for both template models. Since we assume that g-mode eigenfunctions cannot penetrate the solid regions (due to the hard-sphere boundary condition, equation 34), this chemical interface is not relevant for the mode-trapping properties of the models. The chemical transition region between ^{12}C, ^{16}O, and ^{4}He $[-\log(1 - M_r/M_\star) \sim 4.5]$, which is located in the fluid region in both models, also does not have a significant impact on the mode-trapping properties. Thus, mode-trapping properties are almost entirely determined by the presence of the ^{4}He/^{1}H transition, which is located in the fluid external regions, at $-\log(1 - M_r/M_\star) \sim 6$.

By closely inspecting Fig. 6, we conclude that the Brunt–Väisälä and Lamb frequencies for the N and GR cases are similar for the

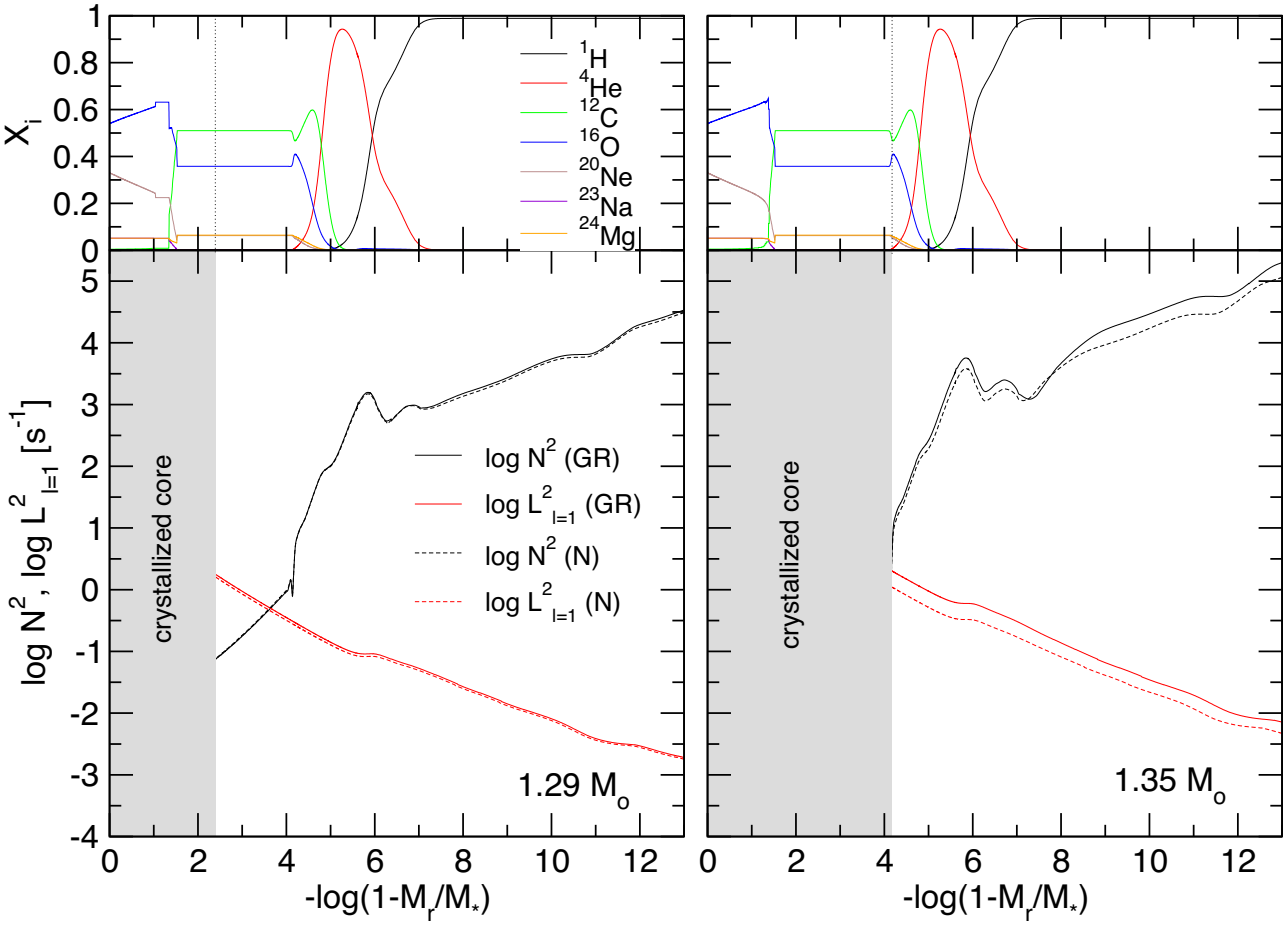

Figure 6. Upper panels: abundances by mass of the different chemical species as a function of the fractional mass, corresponding to the template WD models with masses $M_\star = 1.29\,\mathrm{M}_\odot$ (left) and $M_\star = 1.35\,\mathrm{M}_\odot$ (right), and effective temperature $T_{\rm eff} \sim 12\,000$ K. Lower panels: logarithm of the squared Brunt–Väisälä and Lamb ($\ell = 1$) frequencies for the GR case (solid lines) and the N case (dashed lines). The grey areas correspond to the crystallized core regions, in which g modes cannot propagate.

Downloaded from https://academic.oup.com/mnras/article/524/4/5929/7231806 by guest on 07 August 2023

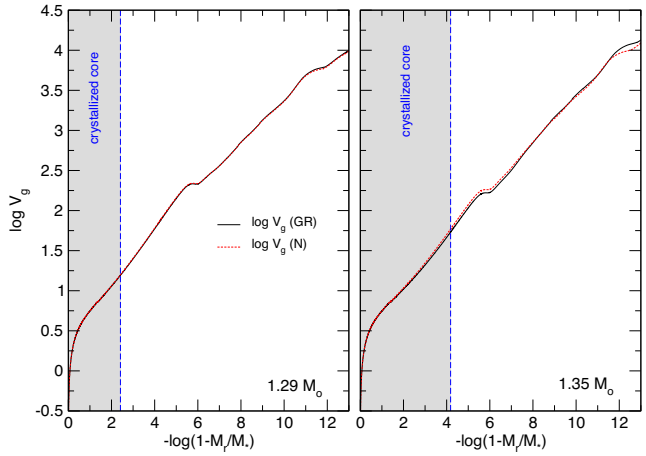

Figure 7. Logarithm of the quantity V_g for the GR case (black solid lines), defined by equation (25), as a function of the fractional mass, corresponding to the template WD models with masses $M_\star = 1.29\,\mathrm{M}_\odot$ (left) and $M_\star = 1.35\,\mathrm{M}_\odot$ (right), and effective temperature $T_{\rm eff} \sim 12\,000$ K. For comparison, we include the function V_g computed for the N case (red dashed lines). The vertical dashed blue line indicates the location of the boundary of the crystallized core region (grey zone).

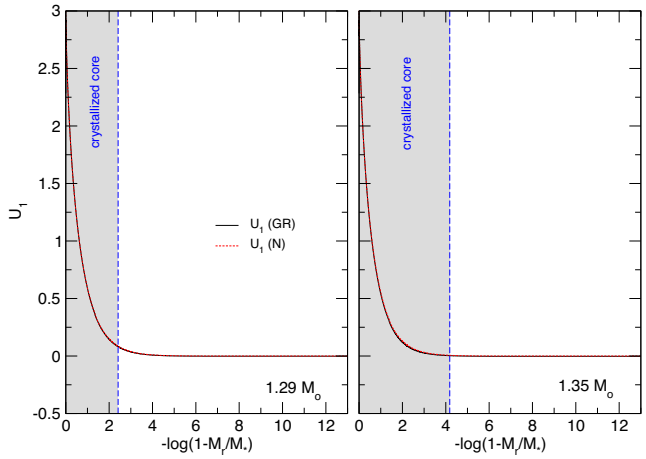

Figure 8. Same as Fig. 7, but for the quantity U_1 (equation 26).

model with $M_\star = 1.29\,\mathrm{M}_\odot$, although they are significantly different for the $M_\star = 1.35\,\mathrm{M}_\odot$ model, with both critical frequencies being higher for the GR case than for the N case. Because of this, it is expected that g-mode frequencies shift to larger values so that all periods experience a global offset towards shorter values in the relativistic case, compared to the Newtonian case. This will be verified with the calculations of the g-mode period spectra in both situations (Section 4.2).

We close this section by comparing the coefficients of the differential equations of the relativistic Cowling approximation with their Newtonian counterparts. In Figs 7–11, we depict with black curves the dimensionless functions V_g, U_1, U_2, C_1, and A^* in the GR case, as defined by equations (25) to (29), along with the same quantities corresponding to the N case (red curves), computed according to their definition (see e.g. Unno et al. 1989). We include the cases of the two template WD models with $M_\star = 1.29\,\mathrm{M}_\odot$ (left-hand panel) and $M_\star = 1.35\,\mathrm{M}_\odot$ (right-hand panel). We marked the crystallized region in each model with a grey area with a dashed blue boundary.

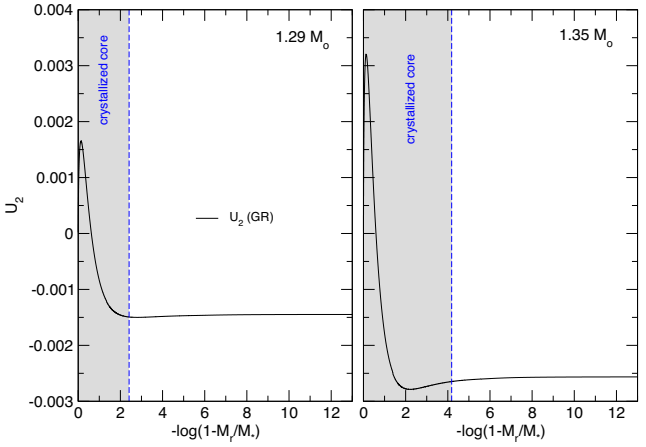

Figure 9. Same as Fig. 7, but for the quantity U_2 (equation 27). Since U_2 has no counterpart in the Newtonian pulsation equations, only the GR case is plotted (black curves).

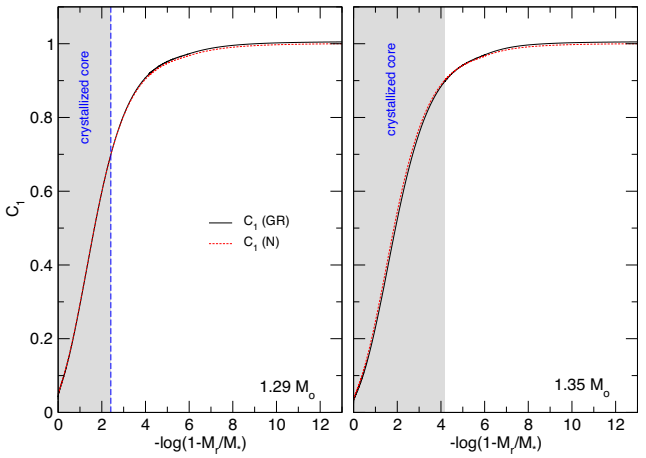

Figure 10. Same as Fig. 7, but for the quantity C_1 (equation 28).

These figures demonstrate that the dimensionless quantities in the GR case are very similar to the ones for the N case, and this is true for both of the representative models. This is not surprising, since the relativistic correction factors ν and λ and their derivatives ν', λ', and ν'', which are included in the calculation of the dimensionless coefficients, are small. For the specific case of A^*, some numerical noise is observed in the core regions. This is irrelevant for the purposes of this investigation, since those regions are contained in the crystallized core and do not affect the g modes, which are prevented from propagating in the solid phase.

4.2 Newtonian and relativistic g-mode period spectra

We computed N and GR non-radial g-mode $\ell = 1$ adiabatic pulsation periods in the range $50\ \mathrm{s} \lesssim \Pi \lesssim 2000\ \mathrm{s}$ using an updated version of the LP-PUL pulsation code that includes the capability to solve the pulsation equations in the relativistic Cowling approximation described in Section 3.1. The N-case pulsation periods were calculated by solving the differential problem of the Newtonian non-radial stellar pulsations (Unno et al. 1989). We emphasize that in the GR case we are using evolutionary WD models calculated in GR with relativistic, second-order Cowling mode pulsations that ignore gravitational (i.e. spacetime) perturbations, while in the N case we are using

Downloaded from https://academic.oup.com/mnras/article/524/4/5929/7231806 by guest on 07 August 2023

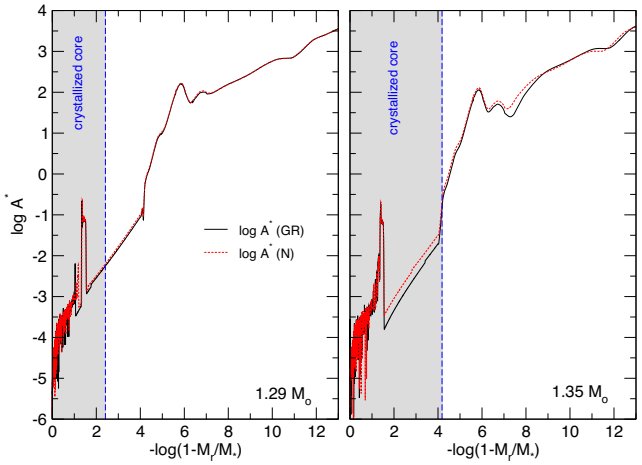

Figure 11. Same as Fig. 7, but for the logarithm of the quantity A^* (equation 29).

evolutionary WD models calculated with Newtonian gravity and Newtonian, fourth-order mode pulsations that include gravitational perturbations.[3] We have also computed Newtonian periods by solving the second-order Newtonian Cowling approximation (Unno et al. 1989). For g modes, these second-order periods are sufficiently similar to the fourth-order periods used in the N case, in that the results are not impacted.

In the analysis below, to study the dependence of the relativistic effects on the stellar mass, we compare the g-mode period spectra calculated according to the N and GR cases for ultra-massive WD models of different stellar masses at effective temperatures typical of the ZZ Ceti instability strip.

Before analysing the behaviour of the periods, we first examine the impact of GR on the period spacing of g modes. According to the asymptotic theory of stellar pulsations, and in the absence of chemical gradients, the pulsation periods of the g modes with high radial order k (long periods) are expected to be uniformly spaced with a constant period separation given by (Tassoul 1980; Tassoul et al. 1990)

$$\Delta\Pi_\ell^{\rm a} = \Pi_0/\sqrt{\ell(\ell+1)}, \tag{35}$$

where

$$\Pi_0 = 2\pi^2\left[\int_{\rm fluid}\frac{N}{r}{\rm d}r\right]^{-1}, \tag{36}$$

with the integral in equation (36) calculated only in the fluid part of the star. Fig. 12 depicts the asymptotic period spacing for the sequences of 1.29, 1.31, 1.33, 1.35, and 1.369 $M_\odot$ WD models in terms of the effective temperature along the ZZ Ceti instability strip. We find that $\Delta\Pi_\ell^{\rm a}$, the asymptotic period spacing, is smaller for the relativistic WD sequences compared to the Newtonian sequences. This is expected, since the asymptotic period spacing is inversely proportional to the integral of the Brunt–Väisälä frequency divided by the radius. Since the Brunt–Väisälä frequency is larger for the relativistic case (see Fig. 6), the integral is larger and its inverse is smaller than in the Newtonian case. The differences of $\Delta\Pi_\ell^{\rm a}$ between the GR and the N cases are larger for higher stellar masses,

[3]This is at variance with the preliminary results presented in Córsico, Althaus & Camisassa (2023), in which Newtonian equations were used for the g modes, with a fully relativistic WD as the background.

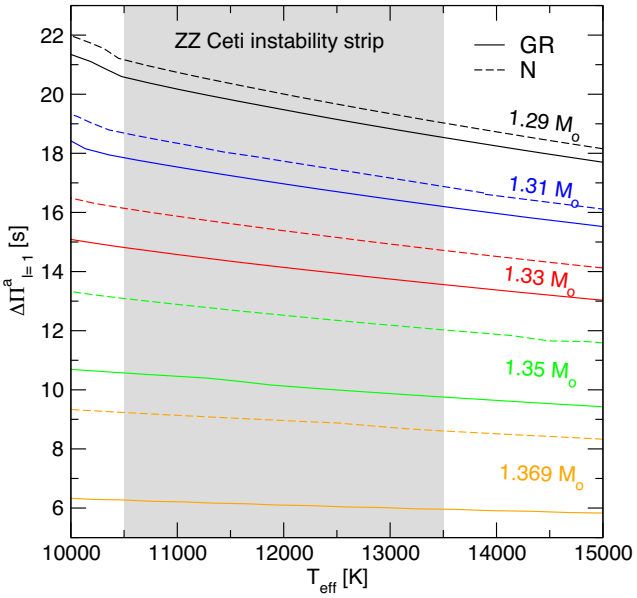

Figure 12. Dipole $\ell = 1$ asymptotic period spacing for ultra-massive WD sequences with different stellar masses for the relativistic (GR) and Newtonian (N) cases in terms of $T_{\rm eff}$ through the whole ZZ Ceti instability strip (light grey area).

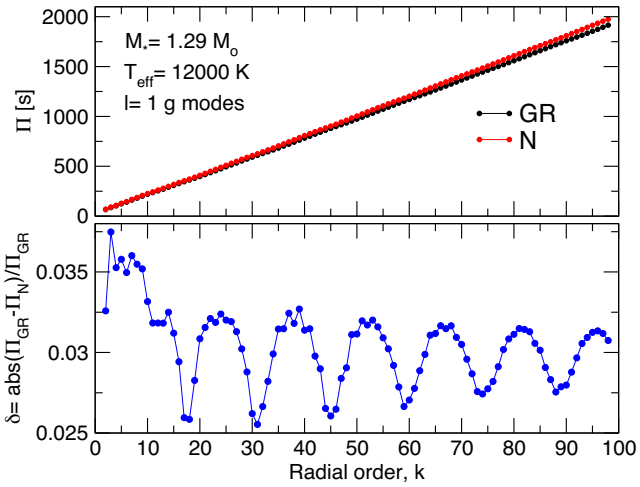

Figure 13. Upper panel: $\ell = 1$ g-mode periods in terms of the radial order (k) for a WD model with $M_\star = 1.29\,M_\odot$ and $T_{\rm eff} \sim 12\,000$ K for the relativistic (GR, black dots) and Newtonian (N, red dots) cases. Lower panel: the absolute value of the relative difference between the periods of the GR and the N cases, $\delta = |\Pi_{\rm GR} - \Pi_{\rm N}|/\Pi_{\rm GR}$ (blue).

reaching a minimum difference of ∼0.6 s (which represents a relative variation in period spacing of ∼3 per cent) for 1.29 $M_\odot$, and a maximum difference of ∼3 s (that constitutes a relative variation of ∼48 per cent) for 1.369 $M_\odot$ for effective temperatures within the ZZ Ceti instability strip.

Since there are substantial differences in the separation of g-mode periods in the GR and N cases, it is natural to expect significant differences in the individual pulsation periods (Π). In the upper panels of Figs 13 and 14, we compare the periods of the GR and N cases for the less massive (1.29 $M_\odot$) and the most massive (1.369 $M_\odot$) WD models considered in this work ($T_{\rm eff} \sim 12\,000$ K). $M_\star = 1.369\,M_\odot$ corresponds to the maximum possible value in

Downloaded from https://academic.oup.com/mnras/article/524/4/5929/7231806 by guest on 07 August 2023

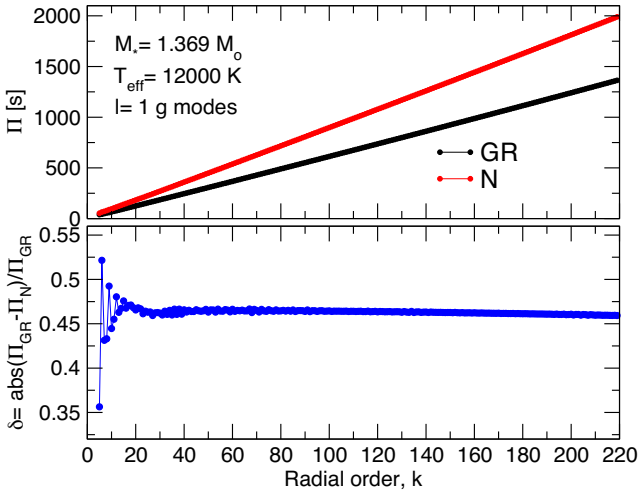

Figure 14. Same as Fig. 13, but for the case of a WD model with $M_\star = 1.369\,\mathrm{M}_\odot$.

the calculations of Althaus et al. (2022), above which the models become unstable with respect to GR effects. It is clear from these figures that the periods in the relativistic case are shorter than those in the Newtonian case, with the absolute differences becoming larger with increasing k. This is mainly due to the structural differences of the equilibrium models in the GR case in relation to the N case (smaller radii and larger gravities characterizing the relativistic WD models, see Fig. 1) and, to a much lesser extent, due to the differences in the relativistic treatment of the pulsations in comparison with the Newtonian one.

To quantify the impact of GR on the period spectrum, we have plotted in the lower panel of each figure the absolute value of the relative differences between the GR periods and the N periods, $\delta = |\Pi_{\rm GR} - \Pi_{\rm N}|/\Pi_{\rm GR}$, versus the radial order. These differences are smaller than ∼0.035 for the less massive model (1.29 $\mathrm{M}_\odot$, Fig. 13), but they become as large as ∼0.5 for the most massive models (1.369 $\mathrm{M}_\odot$, Fig. 14). We conclude that, for ultra-massive WDs with masses in the range $1.29 \leq M_\star/\,\mathrm{M}_\odot \leq 1.369$, the impact of GR on the pulsations is important, resulting in changes from ∼4 per cent to ∼50 per cent in the values of g-mode periods.

Another way to visualize the impact of GR on the pulsation periods is to plot the periods for the GR and N cases in terms of stellar mass. We display in the upper panel of Fig. 15 the periods of selected g modes (with radial orders $k = 5$, 10, 20, 40, and 70) in terms of the stellar mass for the GR and the N cases. In the lower panel, we show the absolute value of the relative difference δ (per cent) between the relativistic and Newtonian periods, as a function of the stellar mass. The relative differences in the periods exhibit an exponential growth with stellar mass, without appreciable dependence on the radial order (see also Figs 13 and 14). The behaviour of δ with the stellar mass visibly mirrors the exponential increase in the relative differences between the relativistic and Newtonian stellar radii and surface gravities, as seen in Fig. 2.

At first glance, the relative differences δ might seem larger than expected, given recent work on periods in average-mass WDs by Boston et al. (2023). For the simple models considered there, it was shown that $\delta \sim z \sim 10^{-4}$ for a WD with $M_\star \approx 0.6\,\mathrm{M}_\odot$. However, considering their fig. 4, it is possible for stars with high central concentrations, such as ultra-massive WDs, that δ can be larger than z, consistent with our present findings. To confirm this, we also carried out pulsational calculations on a simplified stratified

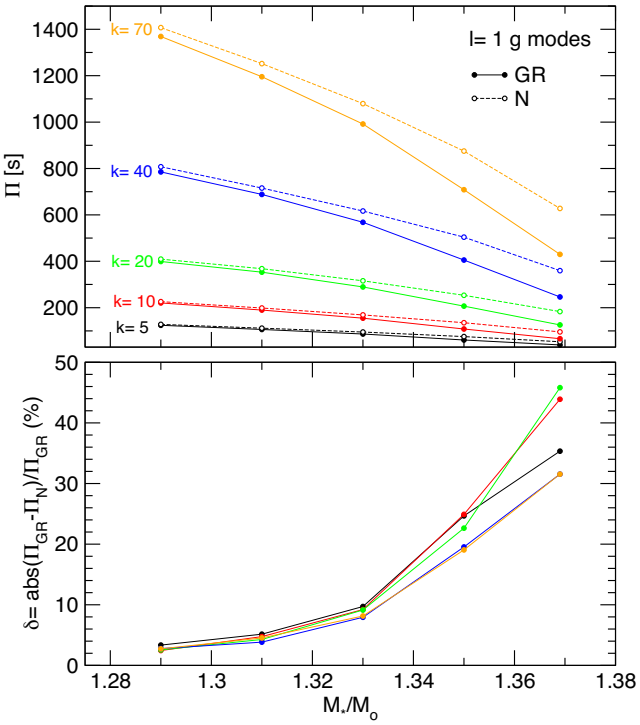

Figure 15. Upper panel: the periods of selected $\ell = 1$ g modes ($k =$ 5, 10, 20, 40, and 70) in terms of the stellar mass, for the GR case (solid lines with filled dots) and the N case (dashed lines with hollow dots). Lower panel: the absolute value of the relative difference δ (per cent) between the relativistic and Newtonian periods, as a function of the stellar mass.

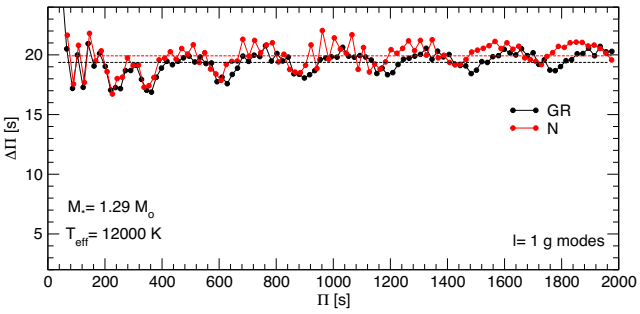

Figure 16. Dipole ($\ell = 1$) forward period spacing ($\Delta\Pi = \Pi_{k+1} - \Pi_k$) versus periods, corresponding to a WD model with $M_\star = 1.29\,\mathrm{M}_\odot$ and $T_{\rm eff} \sim 12\,000$ K for the relativistic case (red), and the Newtonian case (black). The horizontal dashed lines correspond to the asymptotic period spacings for both cases.

Chandrasekhar-type equilibrium model that mimics a ∼1.3 $\mathrm{M}_\odot$ ultra-massive WD, in the case of Newtonian gravity and in the post-Newtonian approximation, following the process in Boston et al. (2023). These calculations and their results are presented in the Appendix B. The comparison of the periods in both cases indicates a relative difference of the order of 10^{-2}, in complete agreement with the results obtained here for our WD models of 1.29 and 1.31 $\mathrm{M}_\odot$ (see Figs 13 and 15).

It is interesting to examine how the period spacings versus periods change depending on whether we consider the GR case or the N case. We define the forward period spacing as $\Delta\Pi = \Pi_{k+1} - \Pi_k$. The dipole ($\ell = 1$) forward period spacing in terms of the periods is plotted in Figs 16–20 for WD models with stellar masses between

Downloaded from https://academic.oup.com/mnras/article/524/4/5929/7231806 by guest on 07 August 2023

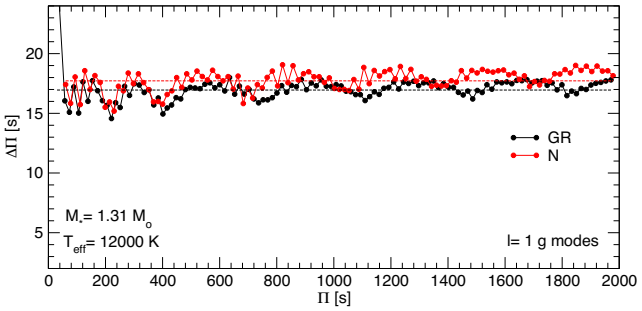

Figure 17. Same as Fig. 16, but for a WD model with $M_\star = 1.31\,\mathrm{M}_\odot$.

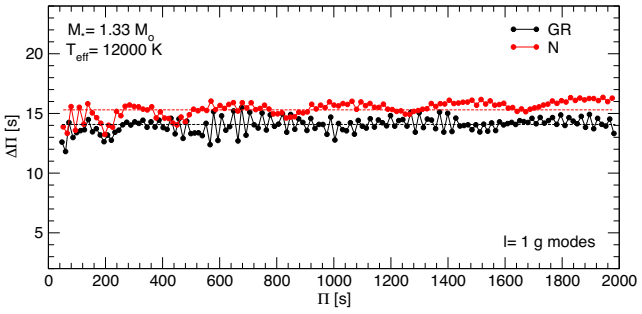

Figure 18. Same as Fig. 16, but for a WD model with $M_\star = 1.33\,\mathrm{M}_\odot$.

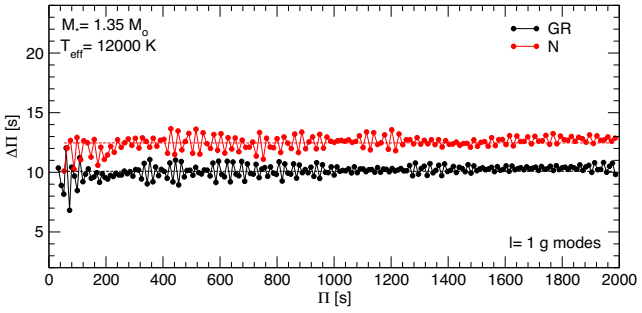

Figure 19. Same as Fig. 16, but for a WD model with $M_\star = 1.35\,\mathrm{M}_\odot$.

1.29 and 1.369 $\mathrm{M}_\odot$ and $T_{\rm eff} = 12\,000$ K. We have adopted the same range in the $y-$axis in order to make the comparison of the results between the different stellar masses clearer. These figures show that, in general, the period spacing is larger in the N case than that in the GR case, and that this difference becomes larger as the stellar mass increases. This is expected based on the behaviour of the asymptotic period spacing (see Fig. 12), which is indicated with horizontal dashed lines.

4.3 The case of the ultra-massive ZZ Ceti star WD J0049−2525

The ultra-massive DA WD star WD J004917.14−252556.81 ($T_{\rm eff} = 13\,020 \pm 460$ K and $\log g = 9.341 \pm 0.036$) is the most massive pulsating WD known to date (Kilic et al. 2023b). It shows only two periods, at ∼209 and ∼221 s, which are insufficient to find a single seismological model that would give us details of its internal structure. Extensive follow-up time-series photometry could allow discoveries of a significant number of additional pulsation periods that would help to probe its interior. Considering the ONe-core WD evolutionary models of Althaus et al. (2022), WD J0049−2525 has $M_\star = 1.283 \pm 0.008$ $\mathrm{M}_\odot$ in the Newtonian gravity, or $M_\star = 1.279 \pm 0.007$ $\mathrm{M}_\odot$ if we adopt the GR treatment. This heavyweight ZZ Ceti, in principle, could be considered as an ideal target to explore the relativistic effects on ultra-massive WD pulsations. However, the difference between the relativistic and Newtonian masses of this target is tiny. A difference of only 0.004 $\mathrm{M}_\odot$ is even smaller than the uncertainties in the mass estimates. This small difference is due to the star being just slightly below the lower mass limit for the relativistic effects to be important.[4]

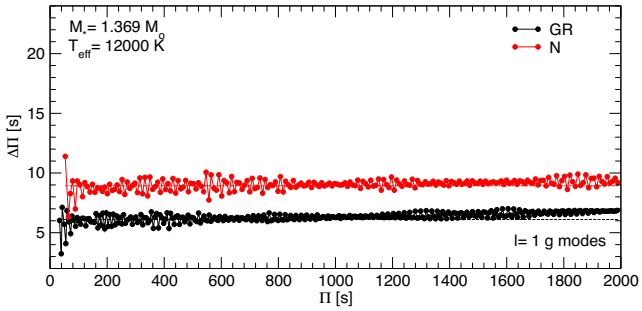

Figure 20. Same as Fig. 16, but for a WD model with $M_\star = 1.369\,\mathrm{M}_\odot$.

Fig. 15 (see also Fig. 16) demonstrates that the effects of the GR on the g-mode periods of WD J0049−2525 are less than ∼1 per cent. Although extremely important for being the most massive pulsating WD star known, WD J0049−2525 is not massive enough for the exploration of the GR effects on WD pulsations. We conclude that, to be able to study the effects of GR on WD pulsations, we have to wait for the discovery and monitoring of even more massive pulsating WDs, especially the ones with $M_\star \gtrsim 1.33\,\mathrm{M}_\odot$.

4.4 Prospects for finding pulsating WDs where GR effects are significant

Fig. 21 shows the masses and effective temperatures for high-probability ($P_{\rm WD} \geq 0.9$) WD candidates with $M_\star \geq 1.3$ $\mathrm{M}_\odot$ in the *Gaia* EDR3 WD sample from Gentile Fusillo et al. (2021) assuming CO cores. Here, we limit the sample to the temperature range near the ZZ Ceti instability strip. The blue and red lines show the boundaries of the instability strip from Vincent et al. (2020) extrapolated to higher masses. There are 78 objects in this sample, including 7 spectroscopically confirmed DA WDs (labelled in the figure) and 6 magnetic or DC WDs. Kilic et al. (2023a) found that only 48 per cent of the $M_\star \approx 1.3$ $\mathrm{M}_\odot$ WDs within 100 pc are DA WDs, with the rest being strongly magnetic (40 per cent of the sample) or WDs with unusual atmospheric compositions (hot DQ, DBA, DC, etc.). Hence, follow-up spectroscopy is required to identify the DA WDs in this sample.

Kilic et al. (2023a) presented time-series photometry for the five DA WDs cooler than 13 000 K in Fig. 21. They did not detect any significant variations in four of the targets, and their observations were inconclusive for J0959−1828. Nevertheless, there are a number of relativistic ultra-massive WD candidates that may fall within the ZZ Ceti instability strip, and therefore may exhibit pulsations. The masses shown here are based on the CO-core evolutionary models; for ONe cores, the masses would be lower on average by 0.04–0.05 $\mathrm{M}_\odot$. Even then, there are nine candidates with $M_\star > 1.35$

[4]That is, $M_\star \sim 1.3\,\mathrm{M}_\odot$, the lower limit of the mass regime of the so-called relativistic ultra-massive WDs (Althaus et al. 2023).

Downloaded from https://academic.oup.com/mnras/article/524/4/5929/7231806 by guest on 07 August 2023

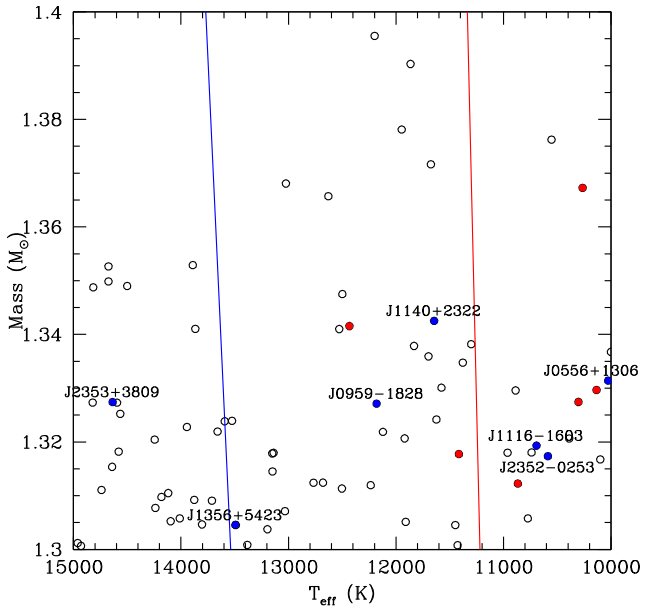

Figure 21. Masses and effective temperatures for high-probability WD candidates with $M_\star \geq 1.3$ M$_\odot$ in the *Gaia* EDR3 WD sample from Gentile Fusillo et al. (2021) assuming CO cores. For ONe cores, the masses would be lower on average by 0.04–0.05 M$_\odot$. The blue and red lines show the empirical boundaries of the ZZ Ceti instability strip from Vincent et al. (2020) extrapolated to higher masses. Blue and red dots show the spectroscopically confirmed DA and DC/magnetic WDs, respectively.

and up to 1.39 M$_\odot$ (assuming a CO core) near the instability strip. If confirmed, such targets would be prime examples of objects where GR effects would have a significant impact on their pulsation properties.

Unfortunately, the observational errors in temperatures and masses of these targets based on *Gaia* photometry and parallaxes (Gentile Fusillo et al. 2021) are too large to effectively identify the best targets for follow-up. For example, 64 of the 78 objects shown here have temperature errors larger than 2000 K, roughly the width of the instability strip, and 62 have errors in mass that are larger than 0.1 M$_\odot$. Hence, further progress on understanding the GR effects on WD pulsation will require spectroscopic and time-series observations of a relatively large sample of candidates to identify genuine pulsating ultra-massive WDs with $M_\star \gtrsim 1.33$ M$_\odot$. In addition, the median G-band magnitude for these 78 objects is 20.25 mag. Hence, 4–8 m class telescopes would be needed to confirm pulsating DA WDs in this sample.

5 SUMMARY AND CONCLUSIONS

In this paper, we have assessed for the first time the impact of GR on the g-mode period spectra of ultra-massive ZZ Ceti stars. To this end, we pulsationally analysed fully evolutionary ONe-core ultra-massive WD models with masses from 1.29 to 1.369 M$_\odot$ computed in the frame of GR (Althaus et al. 2022). We employed the LPCODE and LP-PUL evolutionary and pulsation codes, respectively, adapted for relativistic calculations. In particular, for the pulsation analysis, we considered the relativistic Cowling approximation. Our study is consistent with Boston et al. (2023), considering the high central compactness of the stars studied here. The study of pulsating ultra-massive WDs in the context of GR is timely considering the increasing rate of discovery of very high mass objects (e.g. Hollands et al. 2020; Kilic et al. 2020, 2021, 2023a; Caiazzo et al. 2021; Torres et al. 2022), the discovery of the ZZ Ceti WD J004917.14−252556.81 (the most massive pulsating WD currently known; Kilic et al. 2023b), and the possibility of finding even more massive pulsating objects in the near future. This is particularly relevant in view of the space-based surveys like *TESS* and *ULTRASAT* and wide-field ground-based surveys like the LSST and BlackGEM.

We find that the Brunt–Väisälä and Lamb frequencies are larger for the relativistic case compared to the Newtonian case, as a result of relativistic models having smaller radii and higher gravities. This has the important consequence that the typical separation between consecutive g-mode periods is smaller in the relativistic case than that in the Newtonian computations, with percentage differences of up to 48 per cent in the case of the most massive model (1.369 M$_\odot$). We assessed the dipole period spectrum of g modes of our ultra-massive WD models for the Newtonian and the relativistic cases, and found that the periods in the GR case are shorter than those in the Newtonian computations. In particular, for the less massive model (1.29 M$_\odot$), these relative differences are smaller than ∼0.035, but the variations reach values as large as ∼0.5 for the most massive model (1.369 M$_\odot$).

We conclude that, for ultra-massive DA WD models with masses in the range that we have considered in this paper ($1.29 \leq M_\star/\,\mathrm{M}_\odot \leq 1.369$) and effective temperatures typical of the ZZ Ceti instability strip, GR does matter in computing the adiabatic g-mode pulsations, resulting in periods that are between ∼4 and ∼50 per cent shorter, depending on the stellar mass, when a relativistic treatment is adopted instead of a Newtonian one. This suggests that the effects of GR on the structure and pulsations of WDs with masses $\gtrsim$1.29 M$_\odot$ cannot be ignored in asteroseismological analysis of ultra-massive ZZ Ceti stars and likely other classes of pulsating WDs.

ACKNOWLEDGEMENTS

We wish to thank the suggestions and comments of an anonymous referee that improved the original version of this work. Part of this work was supported by AGENCIA through the Programa de Modernización Tecnológica BID 1728/OC-AR, by the PIP 112-200801-00940 grant from CONICET, by the National Science Foundation under grants AST-2205736 and PHY-2110335, by the National Aeronautics and Space Administration under grant 80NSSC22K0479, and by the US DOE under contract DE-AC05-00OR22725. ST acknowledges support from MINECO under the PID2020-117252GB-I00 grant and by the AGAUR/Generalitat de Catalunya grant SGR-386/2021. MEC acknowledges grant RYC2021-032721-I, funded by MCIN/AEI/10.13039/501100011033 and by the European Union NextGenerationEU/PRTR. This research has made use of NASA Astrophysics Data System.

DATA AVAILABILITY

The data underlying this article are available upon request.

REFERENCES

Althaus L. G., Córsico A. H., Isern J., García-Berro E., 2010, A&AR, 18, 471
Althaus L. G. et al., 2021, A&A, 646, A30
Althaus L. G., Camisassa M. E., Torres S., Battich T., Córsico A. H., Rebassa-Mansergas A., Raddi R., 2022, A&A, 668, A58

Downloaded from https://academic.oup.com/mnras/article/524/4/5929/7231806 by guest on 07 August 2023

Althaus L. G., Córsico A. H., Camisassa M. E., Torres S., Gil-Pons P., Rebassa-Mansergas A., Raddi R., 2023, MNRAS, 523, 4492
Andersson N., Kokkotas K. D., Schutz B. F., 1995, MNRAS, 274, 1039
Bédard A., Bergeron P., Fontaine G., 2017, ApJ, 848, 11
Ben-Ami S. et al., 2022, in den Herder J.-W. A., Nikzad S., Nakazawa K., eds, Proc. SPIE Conf. Ser. Vol. 12181, Space Telescopes and Instrumentation 2022: Ultraviolet to Gamma Ray. SPIE, Bellingham, p. 1218105
Borucki W. J. et al., 2010, Science, 327, 977
Boston S. R., 2022, PhD thesis, University of North Carolina at Chapel Hill
Boston S. R., Evans C. R., Clemens J. C., 2023, ApJ, 952, 87
Brassard P., Fontaine G., Wesemael F., Kawaler S. D., Tassoul M., 1991, ApJ, 367, 601
Caiazzo I. et al., 2021, Nature, 595, 39
Camisassa M. E. et al., 2019, A&A, 625, A87
Camisassa M. E., Althaus L. G., Koester D., Torres S., Gil-Pons P., Córsico A. H., 2022, MNRAS, 511, 5198
Carvalho G. A., Marinho R. M., Malheiro M., 2018, Gen. Relativ. Gravit., 50, 38
Chandrasekhar S., Detweiler S., 1975, Proc. R. Soc. A, 344, 441
Chidester M. T., Farag E., Timmes F. X., 2022, ApJ, 935, 21
Cohen J. M., Lapidus A., Cameron A. G. W., 1969, Ap&SS, 5, 113
Córsico A. H., 2020, Frontiers Astron. Space Sci., 7, 47
Córsico A. H., 2022, Bol. Asociación Argentina Astron., 63, 48
Córsico A. H., Althaus L. G., 2006, A&A, 454, 863
Córsico A. H., Althaus L. G., Miller Bertolami M. M., Kepler S. O., 2019, A&AR, 27, 7
Córsico A. H., Althaus L. G., Camisassa M. E., 2023, preprint (arXiv:2302.04100)
Cowling T. G., 1941, MNRAS, 101, 367
Curd B., Gianninas A., Bell K. J., Kilic M., Romero A. D., Allende Prieto C., Winget D. E., Winget K. I., 2017, MNRAS, 468, 239
Curtis A. R., 1950, Proc. R. Soc. A, 200, 248
Cutler C., 1991, ApJ, 374, 248
Cutler C., Lindblom L., 1992, ApJ, 385, 630
Detweiler S., Lindblom L., 1985, ApJ, 292, 12
Dziembowski W. A., 1971, Acta Astron., 21, 289
Fackerell E. D., 1971, ApJ, 166, 197
Faulkner J., Gribbin J. R., 1968, Nature, 218, 734
Flores C. V., Hall Z. B., Jaikumar P., 2017, Phys. Rev. C, 96, 065803
Fontaine G., Brassard P., 2008, PASP, 120, 1043
Gagné J., Fontaine G., Simon A., Faherty J. K., 2018, ApJ, 861, L13
Gentile Fusillo N. P. et al., 2021, MNRAS, 508, 3877
Giammichele N., Charpinet S., Brassard P., 2022, Frontiers Astron. Space Sci., 9, 879045
Groot P. J. et al., 2022, in Marshall H. K., Spyromilio J., Usuda T., eds, Proc. SPIE Conf. Ser. Vol. 12182, Ground-based and Airborne Telescopes IX. SPIE, Bellingham, p. 121821V
Hamada T., Salpeter E. E., 1961, ApJ, 134, 683
Hermes J. J., Kepler S. O., Castanheira B. G., Gianninas A., Winget D. E., Montgomery M. H., Brown W. R., Harrold S. T., 2013, ApJ, 771, L2
Hewish A., Bell S. J., Pilkington J. D. H., Scott P. F., Collins R. A., 1968, Nature, 217, 709
Hollands M. A. et al., 2020, Nat. Astron., 4, 663
Howell S. B. et al., 2014, PASP, 126, 398
Ipser J. R., Thorne K. S., 1973, ApJ, 181, 181
Kanaan A., Kepler S. O., Giovannini O., Diaz M., 1992, ApJ, 390, L89
Kilic M., Bergeron P., Kosakowski A., Brown W. R., Agüeros M. A., Blouin S., 2020, ApJ, 898, 84
Kilic M., Bergeron P., Blouin S., Bédard A., 2021, MNRAS, 503, 5397
Kilic M. et al., 2023a, MNRAS, 518, 2341
Kilic M., Córsico A. H., Moss A. G., Jewett G., De Gerónimo F. C., Althaus L. G., 2023b, MNRAS, 522, 2181
Kippenhahn R., Weigert A., 1990, Stellar Structure and Evolution. Springer-Verlag, Berlin, Heidelberg
Kumar P., Townsley D. M., 2023, ApJ, 951, 122
Lindblom L., Detweiler S. L., 1983, ApJS, 53, 73
Lindblom L., Splinter R. J., 1989a, ApJ, 345, 925
Lindblom L., Splinter R. J., 1990, ApJ, 348, 198
Lindblom L., Mendell G., Ipser J. R., 1997, Phys. Rev. D, 56, 2118
Maoz D., Mannucci F., Nelemans G., 2014, ARA&A, 52, 107
Mathew A., Nandy M. K., 2017, Res. Astron. Astrophys., 17, 061
McDermott P. N., van Horn H. M., Scholl J. F., 1983, ApJ, 268, 837
McDermott P. N., Hansen C. J., van Horn H. M., Buland R., 1985, ApJ, 297, L37
McDermott P. N., van Horn H. M., Hansen C. J., 1988, ApJ, 325, 725
Meltzer D. W., Thorne K. S., 1966, ApJ, 145, 514
Montgomery M. H., Klumpe E. W., Winget D. E., Wood M. A., 1999, ApJ, 525, 482
Nugent P. E. et al., 2011, Nature, 480, 344
Nunes S. P., Arbañil J. D. V., Malheiro M., 2021, ApJ, 921, 138
Oppenheimer J. R., Volkoff G. M., 1939, Phys. Rev., 55, 374
Poisson E., Will C. M., 2014, Gravity. Cambridge Univ. Press, Cambridge
Regge T., Wheeler J. A., 1957, Phys. Rev., 108, 1063
Ricker G. R. et al., 2014, in Oschmann J. M., Jr, Clampin M., Fazio G. G., MacEwen H. A., eds, Proc. SPIE Conf. Ser. Vol. 9143, Space Telescopes and Instrumentation 2014: Optical, Infrared, and Millimeter Wave. SPIE, Bellingham, p. 914320
Romero A. D. et al., 2022, MNRAS, 511, 1574
Rotondo M., Rueda J. A., Ruffini R., Xue S.-S., 2011, Phys. Rev. D, 84, 084007
Rowan D. M., Tucker M. A., Shappee B. J., Hermes J. J., 2019, MNRAS, 486, 4574
Saio H., 2019, MNRAS, 487, 2177
Siess L., 2007, A&A, 476, 893
Siess L., 2010, A&A, 512, A10
Skilling J., 1968, Nature, 218, 923
Sotani H., Takiwaki T., 2020, Phys. Rev. D, 102, 063025
Tassoul M., 1980, ApJS, 43, 469
Tassoul M., Fontaine G., Winget D. E., 1990, ApJs, 72, 335
Thorne K. S., 1966, ApJ, 144, 201
Thorne K. S., 1967, in Dewitt C., Schatzman E., Véron P., eds, High Energy Astrophysics, Vol. 3, Gordon and Breach Science Publishers, New York, p. 259
Thorne K. S., 1977, ApJ, 212, 825
Thorne K. S., Campolattaro A., 1967, ApJ, 149, 591
Thorne K. S., Ipser J. R., 1968, ApJ, 152, L71
Tolman R. C., 1939, Phys. Rev., 55, 364
Tonetto L., Lugones G., 2020, Phys. Rev. D, 101, 123029
Tooper R. F., 1964, ApJ, 140, 434
Torres S., Canals P., Jiménez-Esteban F. M., Rebassa-Mansergas A., Solano E., 2022, MNRAS, 511, 5462
Unno W., Osaki Y., Ando H., Saio H., Shibahashi H., 1989, Nonradial Oscillations of Stars, 2nd edn. University of Tokyo Press, Tokyo
Vincent O., Bergeron P., Lafrenière D., 2020, AJ, 160, 252
Winget D. E., Kepler S. O., 2008, ARA&A, 46, 157
Yoshida S., Lee U., 2002, A&A, 395, 201
Zheng Z.-Y., Sun T.-T., Chen H., Wei J.-B., Burgio G. F., Schulze H. J., 2023, Phys. Rev. D, 107, 103048

APPENDIX A: RELATIVISTIC EXPRESSION FOR THE BRUNT–VÄISÄLÄ FREQUENCY IN THE 'MODIFIED LEDOUX' PRESCRIPTION

We start from the relativistic expression for the Brunt–Väisälä frequency, obtained according to its definition (equation 18). This expression can be derived by considering slight buoyant perturbations of a fluid packet within the stellar medium, as detailed in Boston (2022). In the GR case, N^2 is given by

$$N^2 = -\frac{c^2}{2}\nu' \mathrm{e}^{-\lambda}\left[\frac{1}{\rho + P/c^2}\left(\frac{\mathrm{d}\rho}{\mathrm{d}r}\right) - \frac{1}{\Gamma_1 P}\left(\frac{\mathrm{d}P}{\mathrm{d}r}\right)\right], \tag{A1}$$

which reduces to the Newtonian result in the limit $c \to \infty$. In what follows, we will derive expressions for the first and second members inside the brackets of equation (A1). In the Newtonian case, if stellar

Downloaded from https://academic.oup.com/mnras/article/524/4/5929/7231806 by guest on 07 August 2023

plasma is composed by M atomic species with fractional abundances X_i, the equation of state can be written as

$$P = P(\rho, T, \{X_i\}), \tag{A2}$$

where $i = 1, \cdots, M-1$, and $\sum_{i=1}^{M-1} X_i + X_M = 1$. In the relativistic case, we have, instead,

$$P = P(n, T, \{X_i\}), \tag{A3}$$

where n is the baryonic number density. Following Brassard et al. (1991), we can differentiate P from equation (A3) and write

$$\mathrm{d}\ln P = \chi_n \mathrm{d}\ln n + \chi_T \mathrm{d}\ln T + \sum_{i=1}^{M-1} \chi_{X_i} \mathrm{d}\ln X_i, \tag{A4}$$

where χ_T, χ_n, and χ_{X_i} are given by equation (21). Now, from equation (A4) we have

$$\frac{\mathrm{d}\ln n}{\mathrm{d}\ln P} = \frac{1}{\chi_n} - \frac{\chi_T}{\chi_n}\nabla - \frac{1}{\chi_n}\sum_{i=1}^{M-1} \chi_{X_i} \frac{\mathrm{d}\ln X_i}{\mathrm{d}\ln P}. \tag{A5}$$

The relativistic adiabatic exponent, Γ_1, is defined as

$$\Gamma_1 = \left(\frac{\partial \ln P}{\partial \ln n}\right)_{\rm ad}. \tag{A6}$$

Following Kippenhahn & Weigert (1990, equations 6.6 and 13.24), we can write

$$\Gamma_1 = \frac{1}{\alpha - \delta\nabla}, \tag{A7}$$

where

$$\alpha = \left(\frac{\mathrm{d}\ln\rho}{\mathrm{d}\ln P}\right)_T, \quad \delta = -\left(\frac{\mathrm{d}\ln\rho}{\mathrm{d}\ln T}\right)_P. \tag{A8}$$

From the definition of χ_T and χ_n (equation 21), and using the property of the partial derivatives $(\partial f/\partial y)_x = -(\partial f/\partial x)_y \cdot (\partial x/\partial y)_f$, we have

$$\alpha = \frac{1}{\chi_n}, \quad \delta = \frac{\chi_T}{\chi_n}, \tag{A9}$$

so that Γ_1 can be written as

$$\frac{1}{\Gamma_1} = \frac{(1 - \chi_T \nabla_{\rm ad})}{\chi_n}. \tag{A10}$$

The first law of thermodynamics in GR can be written (equation 2.12 of Thorne 1967, converted to standard, non-geometrized units) as

$$\mathrm{d}\rho = \left[\frac{\rho + P/c^2}{n}\right]\mathrm{d}n + \frac{T}{c^2} n\,\mathrm{d}s + \sum_k \mu_k n\,\mathrm{d}X_k, \tag{A11}$$

where T, s, and μ_k are the temperature, the entropy per baryon, and the nuclear chemical potential of the species k, respectively.

If we now assume isentropic changes ($\mathrm{d}s = 0$) and suppose that the abundances of the nuclear species do not change ($\mathrm{d}X_k = 0$; equation 2.14 of Thorne 1967), then by differentiating with respect to r, we finally have

$$\frac{\mathrm{d}\rho}{\mathrm{d}r} = \left[\frac{\rho + P/c^2}{n}\right]\frac{\mathrm{d}n}{\mathrm{d}r}. \tag{A12}$$

Equation (A12) can be written as

$$\frac{1}{\rho + P/c^2}\left(\frac{\mathrm{d}\rho}{\mathrm{d}r}\right) = \frac{1}{n}\frac{\mathrm{d}n}{\mathrm{d}r}. \tag{A13}$$

Substituting equation (A13) in equation (A1), using the static TOV (Tolman-Oppenheimer-Volkoff) equation of GR (Oppenheimer & Volkoff 1939; Tolman 1939),

$$\frac{\mathrm{d}P}{\mathrm{d}r} = -\frac{1}{2}\left(\rho + \frac{P}{c^2}\right)c^2\nu', \tag{A14}$$

and employing equations (A5) and (A10), we obtain

$$N^2 = \left(\frac{1}{2}c^2\nu'\right)^2 \mathrm{e}^{-\lambda}\left(\frac{\rho + P/c^2}{P}\right)\frac{\chi_T}{\chi_n} \times \left[\nabla_{\rm ad} - \nabla - \frac{1}{\chi_T}\sum_{i=1}^{M-1}\chi_{X_i}\frac{\mathrm{d}\ln Xi}{\mathrm{d}\ln P}\right], \tag{A15}$$

where the last term inside the brackets is the Ledoux term B (equation 20). Thus, we finally obtain

$$N^2 = \left(\frac{1}{2}c^2\nu'\right)^2 \mathrm{e}^{-\lambda}\left(\frac{\rho + P/c^2}{P}\right)\frac{\chi_T}{\chi_n}\left[\nabla_{\rm ad} - \nabla + B\right]. \tag{A16}$$

APPENDIX B: VALIDATION WITH A TOY MODEL BASED ON CHANDRASEKHAR'S MODELS

As validation of the results presented in this paper, in particular the size of the relative difference in the periods, we have carried out pulsation calculations on a toy model based on Chandrasekhar's models, with a stellar mass $M_\star \sim 1.3\,\mathrm{M}_\odot$. This model has a cold degenerate-electron equation of state featuring a near-surface chemical transition from $\mu_e = 2$ to $\mu_e = 1$, simulating a surface H layer. Thus, this simple model mimics the structure of a stratified realistic ultra-massive WD model. Following the post-Newtonian method described in Boston et al. (2023), we have compared the fourth-order non-radial Newtonian pulsations to the non-radial GR pulsations for this toy model for several g, f, and p modes with low radial orders k for harmonic degrees $\ell = 1, 2$, and 3. We show the results in Table B1. The relative differences we obtain for g modes are, on average, $\sim 2.65 \times 10^{-2}$ (column 4), which is consistent with the results shown in Figs 13 and 15 for the cases of ultra-massive WD models with $M_\star = 1.29\,\mathrm{M}_\odot$ and $M_\star = 1.31\,\mathrm{M}_\odot$, respectively.

Downloaded from https://academic.oup.com/mnras/article/524/4/5929/7231806 by guest on 07 August 2023

Table B1. Periods for several low-order p, f, and g modes corresponding to the Newtonian gravity computations (column 2) and the GR computations (column 3) for a stratified degenerate-electron gas model, both with $M_\star = 1.299\,66\ \mathrm{M}_\odot$. The Newtonian model uses $y_0 = 6.385$, with $z = 6.6012 \times 10^{-4}$, while the GR model uses $y_0 = 6.779$, with $z = 6.3047 \times 10^{-4}$. Column 3 gives the relative difference, which is commensurate with those in Fig. 13.

Mode$_{\ell,k}$	Newtonian Π (s)	Post-Newtonian Π (s)	Rel. diff.
$p_{1,1}$	1.049 5784	0.978 2581	1.52×10^{-3}
$g_{1,1}$	16.267 5050	14.786 5834	2.66×10^{-2}
$g_{1,2}$	35.751 5552	32.493 2485	2.67×10^{-2}
$g_{1,3}$	54.426 4093	49.468 6549	2.67×10^{-2}
$g_{1,4}$	72.917 4383	66.277 8687	2.66×10^{-2}
$g_{1,5}$	91.335 5203	83.021 1550	2.66×10^{-2}
$g_{1,6}$	109.716 9819	99.731 3589	2.66×10^{-2}
$g_{1,7}$	128.077 3819	116.422 5439	2.66×10^{-2}
$g_{1,8}$	146.424 5279	133.101 7651	2.65×10^{-2}
f_2	1.290 9440	1.191 5768	1.12×10^{-2}
$g_{2,1}$	9.416 4937	8.560 7991	2.64×10^{-2}
$g_{2,2}$	20.682 5679	18.800 0960	2.66×10^{-2}
$g_{2,3}$	31.477 1109	28.612 8454	2.66×10^{-2}
$g_{2,4}$	42.164 2251	38.328 3552	2.65×10^{-2}
$g_{2,5}$	52.808 3359	48.004 9281	2.65×10^{-2}
$g_{2,6}$	63.430 6072	57.661 7194	2.65×10^{-2}
$g_{2,7}$	74.040 1429	67.306 9695	2.65×10^{-2}
$g_{2,8}$	84.641 5378	76.944 8380	2.65×10^{-2}
f_3	1.079 6099	1.000 3529	7.39×10^{-3}
$g_{3,1}$	6.682 8617	6.077 1126	2.62×10^{-2}
$g_{3,2}$	14.664 7687	13.332 3883	2.64×10^{-2}
$g_{3,3}$	22.308 7624	20.281 5701	2.64×10^{-2}
$g_{3,4}$	29.875 4567	27.160 6785	2.64×10^{-2}
$g_{3,5}$	37.410 8454	34.011 3796	2.64×10^{-2}
$g_{3,6}$	44.930 0978	40.847 4210	2.64×10^{-2}
$g_{3,7}$	52.439 7798	47.674 7566	2.64×10^{-2}
$g_{3,8}$	59.943 2319	54.496 4175	2.64×10^{-2}

This paper has been typeset from a TEX/LATEX file prepared by the author.

Downloaded from https://academic.oup.com/mnras/article/524/4/5929/7231806 by guest on 07 August 2023

© 2023 The Author(s)
Published by Oxford University Press on behalf of Royal Astronomical Society